Quantification of the EEG of full-term newborns

Hansen, H.H.G.

Award date:
2005

Eindhoven University of Technology
Faculty of Applied Physics

Máxima Medical Center in Veldhoven
Department of Clinical Physics

Quantification of the EEG of full-term newborns

Master's thesis

H.H.G. Hansen

Jan-Dec 2005

MRL/KFM 2005-04

Supervisors

Ir. C.H.L. Peters

Prof.Dr.Ir. P.F.F. Wijn

Abstract

This report describes the first steps towards an automatic EEG based monitoring system for brain function of full-term newborns by using quantitatively mathematically defined parameters.
First, an algorithm for the classification of the background pattern of the EEG has been developed. The background pattern is known to correlate with the prognosis of a child. On basis of the background pattern full-term newborns can be categorized in three groups: newborns with a severe prognosis, newborns with a healthy prognosis and in between, a large group of newborns with an unclear prognosis. The background pattern usually observed for the last group is a burst-suppression pattern, which consists of alternating periods of high and low amplitude, called burst and suppression, or burst and interburst interval, respectively. It is believed that a separate analysis of burst and suppression periods might provide parameters that are capable of distinguishing the children with the worst outcome from those with a less severe outcome. Therefore first an algorithm that automatically separates bursts from interburst intervals has been developed. A sensitivity of 90% and a positive predictive value of 80% was reached when comparing the results of the algorithm to the annotations of an expert on EEG signals of newborns.
Next, a toolbox was developed in Matlab for the separate analysis of these burst and interburst intervals in the time and frequency domain, and a number of parameters for the quantification of these periods has been defined and calculated. Their suitability for monitoring purposes has been discussed. Parameters expected to be suitable are the percentage of time occupied by bursts, the average burstlength and interburst interval length, the average spectral edge, the average peak frequency and the relative amount of delta power present in bursts. Also a pair of parameters that represent the asymmetry in the posterior and anterior areas of the brain have been defined.

Acknowledgements

I would like to thank all the people that supported me during the fulfillment of my graduation project in the past year. First of all I would like to thank Ir. Chris Peters for being my supervisor and for helping me out in 'emergency' situations. I would also like to thank Prof. Dr. Ir. Pieter Wijn for teaching me how to deal with presentations and for his criticism.
In particular I would like to thank dr.Jaco Pasman, Ad Smets and dr. Peter Andriessen for their efforts and time. Despite of my never ending series of questions and demands they were always willing to help me.
I'm also grateful for the help and advises I received from the clinical physicists in training Ir. J.van den Tillaart and Dr. Ir. C.van Pul. Special thanks go to Rian, who accompanied me almost 24 hours a day. I really enjoyed your company.
Furthermore I would like to thank all the students I've worked with during the past year: Rik, Joyce, Charlotte, Homme-Auke, Taco, Ilham, and Paul. It was a pleasure working with you!
And finally and most important I would like to thank Pauline, my parents and friends for their unlimited support. Without you it wouldn't have been possible to succeed!

Contents

Chapter 1

Introduction

Every birth is a miracle. In many cases however complications arise with birth for the newborn child. In some of these cases children are born prematurely. As a consequence of the prematurity these infants are born with underdeveloped and malfunctioning organs with all its consequences. In other cases complications arising with labor, like asphyxia, endanger the newborn's life. In the Máxima Medical Center located in Veldhoven an intensive care department especially equipped for medical assistance of these newborns has been established. This neonatal intensive care unit(NICU) is one of the ten NICU's in the Netherlands. The establishment of NICU's and the research in the field of neonatology during the past decennia has led to an enormous increase of knowledge, of methods of treatment, and of technology. As a consequence the life chances of prematures and full-term newborns have increased tremendously. Nevertheless there is still a large group of newborns, that does not survive, or has to live with severe and less severe disabilities. To help these children, additional clinical information is required. One of the sources that is expected to provide this additional information and that has not already been fully exploited, is the brain. The brain can be regarded as the control center of the human body. If it is possible to determine the degree of functioning of the brain, new knowledge can be obtained, and new techniques and methods of treatment can be developed.
This project will focus on the electroencephalogram (EEG), as a visualization technique of brain functioning and development of the neonatal brain. The EEG is a visual representation of the electrical activity primarily generated in the cortex of the brain. The neonatal EEG is considered to provide a large amount of information, however it is still not clear how this information should be interpreted. Until now, neonatal EEG registrations have mostly been described qualitatively. This qualitative description has shown that a number of features of the neonatal EEG is likely to be correlated with the life chances of the newborn. However, because of the rather vague definition of these features and the large variability of the neonatal EEG signal, interpretation is subjective. Objective definitions are necessary to come to a better understanding of the neonatal EEG.
The focus of this project will therefore be a quantitative description of the neonatal EEG by mathematically defined parameters, that are expected to correlate with the clinical outcome. This project starts by concentrating on the quantification of the full-term EEG, because of the far more complexness of the premature EEG. The project is an initiative of the NICU and the departments of Neonatology, Clinical Neurophysiology and Clinical Physics of the Máxima Medical Center in Veldhoven. The project has been performed in collaboration with the department of Clinical Neurophysiology of the University Medical Center of Nijmegen.

Chapter 2

Theory

2.1 Anatomy and physiology of the brain

In the next few paragraphs the anatomy and physiology of the central nervous system and in more particular the human brain is explained. Because the human central nervous system consists of a complex network of about 100 billion neurons, the first paragraph is dedicated to the neuron, the neuronal network and its functioning.

2.1.1 Neurons

In figure 2.1 a series of neurons is shown. A neuron globally consists of the soma, or cell body, and one or more axons and dendrites. Axons can be considered as the output units of a neuron, they guide information from the soma to the outside of the cell. Dendrites function oppositely, they transport information from outside the cell towards the cell body. This information transport is carried out by means of an action potential.

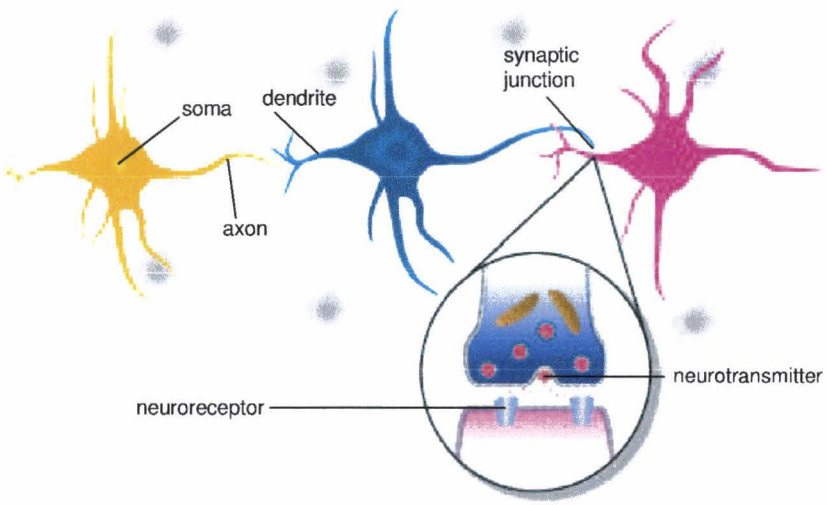

Figure 2.1: *Neurons and their synaptic junctions [21]*

An action potential is a short, spike-shaped fluctuation of the membrane potential, that appears whenever the membrane potential of the neuron rises above a certain threshold potential, about $-50\mu V$. The membrane potential, which is the difference of the potential of the intracellular fluid and the potential of the

extracellular environment, is normally about -70μV. This so-called membrane resting potential is a result of the different concentrations of positively and negatively charged ions, mainly K^+, Na^+ and Cl^- ions, present on the in- and outside of the cell. The negative potential is automatically maintained by an equilibrium of electrical and diffusive forces. The equilibrium can be disturbed by environmental stimuli, for example light, chemicals, pressure etcetera, that cause a temporary change of the permeability of the membrane. Due to this the membrane potential can become less negative. If the potential rises above the aforementioned threshold, voltage triggered gates open in the membrane, that first cause a passive inflow of sodium, the upward flank of the spike-shape, and afterwards an outflow of potassium, the downward flank of the spike. After the generation of an action potential the membrane resting potential and the normal concentrations of potassium and sodium on the in and outside of the cell are restored through active transport by a mechanism called the K^+-Na^+ pump. Because the concentration change of the ions always takes place in the same way, the shape and duration of an action potential are the same for every action potential.
An action potential, which can be generated at any location of the neuron, propagates actively along the cell membrane and via an axon to one or more synaptic junctions. The axon is sometimes covered with an insulating layer called a myelin sheath. This layer is interrupted by nodes, short parts not covered by the myelin sheath. The presence of the myelin sheath enables a faster propagation of action potentials by jumping from node to node. A myelin sheath is usually observed in axons that have to transport information to distant synaptic junctions. Synaptic junctions form the link of neurons with other neurons, as shown in figure 2.1. When an action potential reaches a synaptic junction, a small amount of a chemical substance, named neurotransmitter, is released by the sending axon. This neurotransmitter acts upon a small part of the membrane of the receiving dendrite, the receptor, and changes the membrane's permeability at that area for specific ions. Due to this, ions will start to flow in and out of the intracellular space, the chemical composition will change, and the membrane potential in the dendrite increases (hyperpolarizes), or decreases (depolarizes) temporarily. This might then lead to the generation of a new action potential in the receiving neuron. A depolarization of the receiving neuron, is called an excitatory postsynaptic potential, EPSP, a hyperpolarization is known as an inhibitory postsynaptic potential, IPSP.
Each neuron is connected to multiple neurons by a number of synaptic junctions, which enables a high speed information spread over a very large part of the CNS in a short time period.
Neurons are clustered in functional groups called populations. A population is defined as a group of anatomically adjacent neurons, that receives its input from a common source and has one type of output, either excitatory or inhibitory [4]. A population is mostly made up of a large number of interneurons and relatively few projection neurons. Interneurons process and modulate information within the population. Projection neurons forward information to other brain structures, called projecting. These populations are organized in larger structures called nuclei, and columnar layers.
To increase the speed at which information reaches the processing areas of the CNS, that are dedicated to this specific information, neural pathways have been developed. These are shortcuts from one CNS structure to another. These pathways usually consist of elongated myelin insulated neurons. The specific name of a pathway or tract, which connects two parts of the CNS, is a combination of the name of the structure where it starts and the name of the structure where it ends, for instance the cortico-spinal tract is a neural pathway that starts in the cortex and ends in the spinal cord.

2.1.2 Basal parts of the central nervous system

The directions, that are usually used to describe the anatomy of the central nervous system, are rostral and caudal, and ventral and dorsal. As can be observed in figure 2.2, rostral is the direction along the spinal cord towards the nose and caudal is the opposite direction. Ventral and dorsal are directed perpendicularly to the previous ones. As shown in figure 2.2, directions inwards from the rostro-caudal axis are referred to as ventral, and directions outwards from this axis are named dorsal. The basal parts of the central nervous system, CNS, are illustrated in figure 2.2.
When venturing from the most caudal part to the most rostral part of the CNS, the following five main structures are observed: the spinal cord, brainstem, cerebellum, diencephalon, and the cerebral hemispheres.
The main task of the spinal cord is to receive sensory information from the limbs and trunk and to take care of voluntary and autonomous activity of these parts of the body. The spinal cord is built up of gray matter

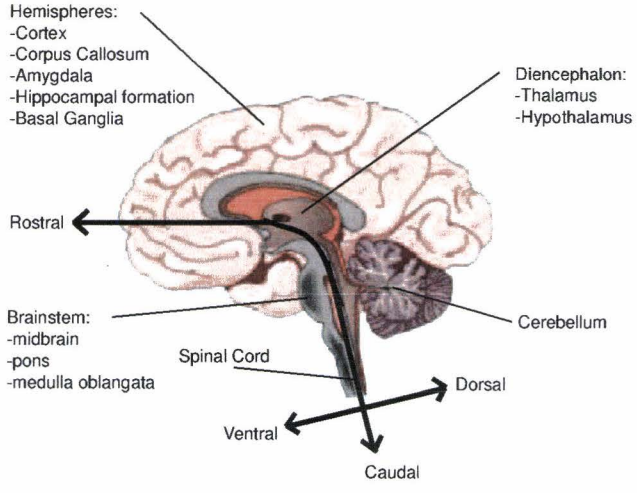

Figure 2.2: *The anatomy of the CNS and the main directions*

and white matter. The gray matter, that has a characteristic butterfly-shape, mainly contains neuronal cell bodies, dendrites and synaptic junctions. The white matter, that surrounds the gray matter, mainly contains myelinated axons. The myelin is responsible for the typical white color.

The brainstem consists of three parts, from caudal to rostral these are: the medulla oblongata, the pons and the midbrain. The general functions of the brainstem are to receive information from the senses in the head, to pass on information from and to other parts of the brain, and to provide control of the activity of muscles in the neck and the head. The latter is mainly carried out in the medulla oblongata, which is anatomically similar to the spinal cord. The second and first task are performed in all three parts of the brainstem. It should be mentioned, that the pons and the medulla also contain centers for the regulation of blood pressure and respiration.

The next part in rostral direction is the cerebellum. The cerebellum is connected to the pons by nerve trunks called the cerebellar peduncles. Through these cerebellar peduncles the cerebellum receives motor information from the cortex, information about posture from the spinal cord and information about balance from the vestibular system. The cerebellum uses this information to make sure posture and balance are maintained by controlling skeletal motor functions.

The diencephalon, that is located rostral to the brainstem and is directly connected to the midbrain, consists of two parts, the thalamus and the hypothalamus. The thalamus is considered to be responsible for the largest part of transport of sensory and motor information from and to the cortex. It is also believed to play an important role in processes of selective attention to stimuli, emotional aspects and the control of level of awareness. The main functions of the hypothalamus are to regulate autonomic functions and hormone secretion. It is also important for the interaction between neuronal and hormonal information processing.

The most rostral and the largest structures of the CNS are the two cerebral hemispheres. These hemispheres are connected by a large nerve trunk, called the corpus callosum. The most superficial layer of the hemispheres is called the cortex. Underneath the cortex white matter is observed. Below the white matter deep structures like the basal ganglia, the hippocampal formation, and the amygdala are found. The hemispheres are believed to contain neuronal structures, that are capable of dealing with the most difficult sensory, motor and cognitive information.

2.1.3 The cortex

As can be observed in figure 2.3A the cerebral cortex consists of sulci ('grooves'), and gyri ('elevations'). The largest sulci 'divide' each hemisphere of the brain in four regions, called lobes. Each lobe is named after its corresponding cranial bone. The line, that divides the cortex in almost equal halves, is called the interhemispheric fissure. It will also be referred to as the sagittal midline. Each lobe can be subdivided into small functional areas, that are dedicated to the performance of specific activities. For instance the 'subgyrus' called precentral gyrus, takes care of primary motor activities. A schematic overview of the functional areas and their corresponding functions is given in figure 2.3B.

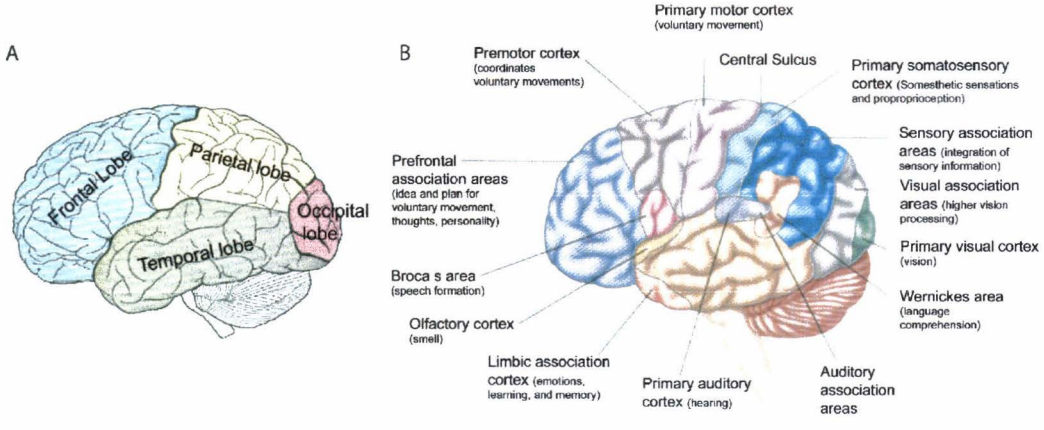

Figure 2.3: *A:the largest four lobes and their naming, B:subareas of the cortex, which are related to specific functions [20]*

Through a microscope the cortex is anatomically organized in six layers. As can be observed in figure 2.4A, these layers are orientated parallel to the surface. Layers 1 to 6 are called lamina molecularis, lamina granularis externa, lamina pyramidalis, lamina granularis interna, lamina ganglionaris, and lamina multiformis respectively.

In general the cortex is made up of two groups of principally different cells: pyramidal cells, that act as projectionneurons and non-pyramidal cells, that function as interneurons. The non-pyramidal cells are often star-shaped and contain a large number of dendrites and a small number of short axons. Through its dendrites the non-pyramidal cell receives information from other parts of the central nervous system or from other non-pyramidal cells. Non-pyramidal cells in the lamina granularis interna are known to receive information directly from the thalamus. The axons are used to pass the modulated information on to other non-pyramidal cells or pyramidal cells via synaptic connections.

The pyramidal cells, whose cellbodies are found in layers 2,3,5 and 6, consist of an apical dendrite, a number of basal dendrites and an axon with possible collateral branches. A pyramidal cell is shown in figure 2.4B. The apical dendrite is a long dendrite, which reaches from the apex (top) of the soma to the lamina molecularis by roughly perpendicularly crossing all cortical layers below. The basal dendrites are shorter dendrites that travel parallel to the surface of the cortex. At the bottom of the pyramidal cell an axon is found with one or more collateral branches. Collateral branches are a kind of mini-axons that form synaptic junctions with basal dendrites of nearby located pyramidal cells. In this way a localized spread of information is created. The main axon projects either onto deeper structures of the CNS or onto columnar layers in other parts of the cortex. The latter is mostly carried out by pyramidal cells, whose somas are located in layers 2 and 3. Pyramidal cells from layer 6 mostly project onto the thalamus. Pyramidal cells from layer 5 usually pass information on to deeper structures like the Basal Ganglia, brainstem and spinal cord. A schematic summary of this information transfer is given in figure 2.5.

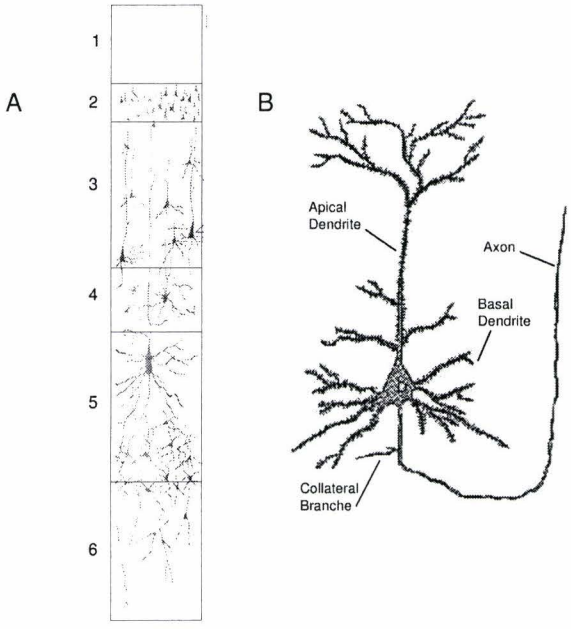

Figure 2.4: *A:the different layers of the cortex [7], B:a schematic representation of a pyramidal cell*

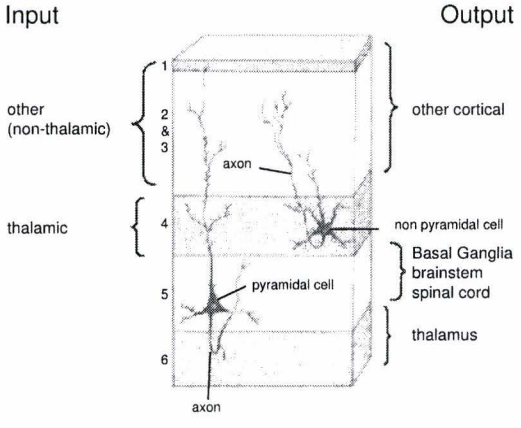

Figure 2.5: *Overview of the input and output of the cortical layers [4]*

2.2 The EEG signal

An EEG signal is a measure of electrical activity in the cortex. The activity is measured via electrodes attached to the scalp. The registration of a human EEG signal was first described in 1929 by the German psychiatrist Hans Berger. The origin of this electrical activity and the international conventions for electrode placement and nomenclature will be discussed in the next paragraphs.

2.2.1 The origin of the EEG signal

The electrical activity measured during an EEG registration, originates from a spatial and temporal summation of electrical dipoles in the cortex of the CNS. The electrical dipoles meant here are in fact small extracellular currents that are evoked in the extracellular fluid of pyramidal cells during the generation of an EPSP or IPSP. The generation of these currents will now be explained for an EPSP. An EPSP is a depolarization of the cell membrane. During this depolarization a small electrical current flows from the presynaptic cell into the postsynaptic cell at the point of the synaptic junction. This current then continues its way through the intercellular space of the axon and leaves the cell again through parts of the membrane adjacent to the synaptic area. Finally, the current continues to flow through the extracellular fluid in opposite direction and completes the circuit. This circuit is shown in figure 2.6. The point at which the current leaves the cell and enters the extracellular fluid can be regarded as source. The point of the synaptic junction can be regarded as sink. From a distance relatively much larger than the distance between sink and source, like the distance from the electrode position to the pyramidal cells, the current circuit can therefore be regarded as an electrical dipole. The source can be interpreted as the positive. The sink can be regarded as the negative.

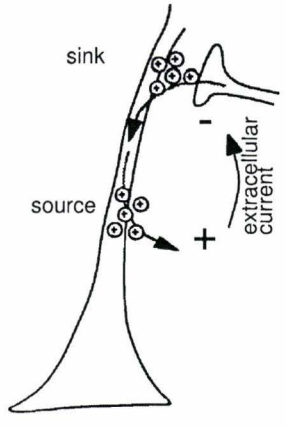

Figure 2.6: *The extracellular dipole generated by the inflow of positively charged ions at the apical dendrite via a synaptic junction*

A single dipole like this, is however much too weak to be detected on the skull, because of the larger amplitude of artifactitious signals that are interfering with the EEG like those summarized in table 2.3. The dipole has a potential difference of only 2.5μV, which is attenuated even further by the resistance of the tissue and the membranes that lay between the dipole and the surface of the skull, as illustrated in figure 2.7. In particular the dura mater, which is one of three membranes that surround the brain, is a membrane with a high resistance.
Normally however amplitudes in the order of $\pm 100\mu$V are measurable, which can be explained as follows. Neuronal populations located in the vicinity of each other are often triggered by a small group of neurons. This means that these populations receive their action potentials almost synchronously. An action potential only lasts about 2ms. The resulting EPSPs or IPSPs, which generate extracellular currents, can last several hundreds of ms. In this way many extracellular currents start running almost simultaneously in a small region of the brain. Because the distance between the electrode and the dipoles is relatively much larger than the distance between the separate dipoles, the number of dipoles N, that appear nearly synchronously in this small region of the cortex, each having a dipole moment $\vec{m}$, can be regarded as one single dipole with a dipole moment of $N * \vec{m}$. Due to the property that the apical dendrites of the pyramidal cells are all aligned perpendicular to the brain's surface, the sum dipole is also directed perpendicular to the surface, which causes it to be measured with an optimal amplitude of $N * |\vec{m}|$ at the surface. This also explains why the high frequent parts of the EEG usually have a much smaller amplitude.

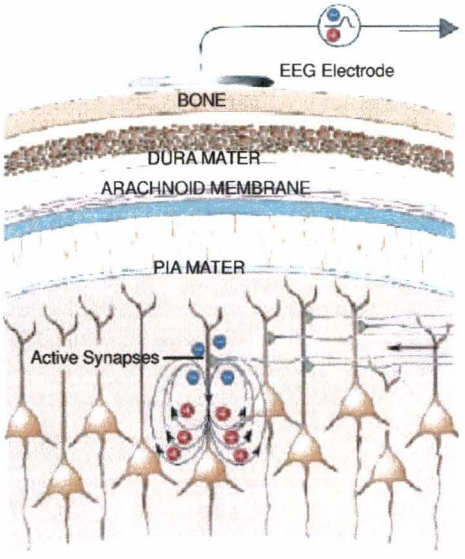

Figure 2.7: *The origin of the EEG signal*

2.2.2 International 10-20 standard

The international 10-20 standard is a convention for the positioning of electrodes and their naming. This standard convention is illustrated in figure 2.8.

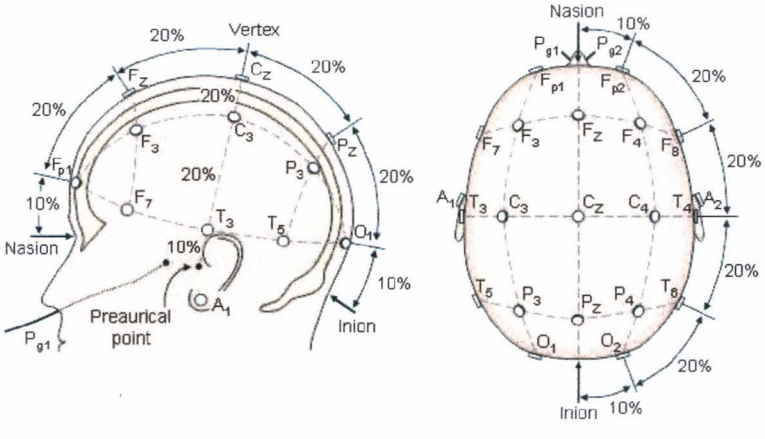

Figure 2.8: *The international 10-20 system: electrode positions and electrode names explained [19]*

As can be observed, the '10-20' is referring to the electrode positions, that are determined with respect to two anatomical reference points. The nasion, which is the delve at the top of the nose, level with the eyes, and the inion, which is the bony lump at the base of the skull on the midline at the back of the head. The electrode positions are determined by drawing imaginary lines between inion and nasion along the surface of the skull in the transverse and median plane. Electrodes are positioned at distances of 10 and 20 percent of these lines as made clear in figure 2.8. In addition, three other electrodes are placed equidistantly from the neighboring points in each hemisphere.
It should be noticed, that the name of the electrodes usually consists of a character part plus a number.

The character part of the electrode name is an abbreviation of the region of the cortex above which the electrode is attached. The number is odd if the electrode is located above the left hemisphere, and even if positioned above the right hemisphere. The further from the median midline, the higher the number. As can be observed the number part is replaced by the character z when the electrode is placed exactly on the sagittal midline.

2.2.3 Electrode derivations

Because one cannot measure absolute potentials, but only differences in potential, an EEG recording requires at least two electrodes, a signal-electrode and a reference. In general more electrodes are used during an EEG recording, and therefore a lot of signal-electrode - reference combinations are possible. A combination of a signal-electrode and its reference is called a derivation. The name of the derivation consists of the hyphenated name of the signal-electrode and the reference, for instance 'O1-O2'.

2.3 The neonatal EEG

The interpretation of an EEG and especially the neonatal EEG is a very difficult task, because the measured signal is stochastic, full of artifacts and cannot be interpreted correctly without knowledge of the patient's condition at the time of the recording. The age of the newborn will show to be important, but also information about the medication received at the time of the recording is of significance.

2.3.1 Interpretation

The interpretation of an EEG registration of a newborn is usually carried out in three steps.
Step one involves the determination of the conceptional age. The conceptional age is defined as the age of the newborn at the moment of the recording, calculated from the first day of the last menstrual period of the mother. It is believed that conceptional age (CA), rather than gestational age (GA), that is the age calculated from birth, is important for the correct interpretation of an EEG registration. The CA is important, because it provides information about the level of brain development that can be expected for a healthy newborn of that CA. Because brain development is reflected in the EEG signal, it is then possible to form an idea of the normal EEG signal that is expected at that CA. Brain development is considered not to be influenced by the event of birth, which means that the EEG registration for a child of a specific CA measured inside the womb is assumed to be similar to the EEG registration measured for the same child at the same CA if it was already born.
Step two involves the determination of the newborn's state of wakefulness or alertness. In general three states are observed for the neonate: wakefulness, active(REM) sleep and quiet(non-REM) sleep. Although the differentiation of all states in the EEG is difficult at conceptional ages before 36 weeks, the knowledge of state is very important for a correct interpretation of the EEG. For instance a discontinuous EEG signal (tracé discontinu) observed during quiet sleep of a healthy neonate of 34 weeks CA can be interpreted as being pathological if it is regarded as a signal originating from the same child during wakefulness. The EEG signal is namely expected to be continuous during the state of wakefulness at this CA. Other non-EEG signals of for instance body movement, eye movement and respiration, often also provide information about state. Therefore these signals are usually also recorded when performing an EEG registration. An EEG registration during which other bioelectrical signals are measured is called a polygraphic EEG registration. The information that can be acquired about state from these other sources is summarized in table 2.1.
The last step of interpretation is evaluating the features of the EEG in context of CA and state. The features of interest are mostly derived from a combination of signal properties in space, time and frequency domain.

2.3.2 Maturation

In this paragraph the 'maturation' of the EEG signal is discussed by presenting the characteristics of the signal for a number of age intervals. These characteristics only account for the healthy neonate. Per interval an overview is given of the states that can be distinguished. Then the background pattern, that is

PCA	State	Eyelids	Eye movement	Body movement	Respiration	EEG
28-32	Mixed	---	---	---	---	Discontinuous
32-36	Awake	Open	Rapid	Present	Irregular	Continuous
	Mixed sleep	Closed	---	---	---	Tracé discontinu
36-42	Awake	Open	Rapid	Slow, sustained	Irregular	Continuous
	Active sleep	Closed	Rapid	Twitches	Irregular	Continuous
	Quiet sleep	Closed	Absent	Absent	Regular	Tracé alternant

Table 2.1: *The various sleep states and the clinical sources on basis of which they can be recognized*

usually observed for these states, is discussed. Finally some characteristic patterns that can be observed for that age and state are described. The definition of 'background pattern' that will be used throughout the rest of this report is: the characterization of the EEG registration on a basis of amplitude characteristics without taking artifacts, epileptic activity and characteristic patterns into account. The different background patterns mentioned in the next paragraph are illustrated in Appendix A.
In the following description of the characteristic patterns the terms delta, theta, alpha and beta activity will be frequently used. These terms refer to specific frequency bands within the spectrum of EEG activity. A schematic overview of the range of frequencies in each band is given in table 2.2. The frequencies, that are usually present in an EEG, range from 0 to 30Hz.

Frequency Band	Frequency Range
delta	<4Hz
theta	4-8Hz
alpha	8-13Hz
beta	13-30Hz

Table 2.2: *The EEG spectral bands and their naming*

25-28 Weeks CA

States: at this age no clear differentiation of states can be made. Only one undifferentiated state exists.
Background: tracé discontinu, which is defined as a signal, characterized by suddenly appearing periods of high amplitude, called bursts, and periods of low amplitude($< 20\mu V$) in between, the interburst intervals (IBIs) [3]. Burst activity is synchronous over both hemispheres. It has been shown that the duration of IBIs and bursts is directly proportional to the degree of prematurity [3]. It should however be kept in mind, that prematurity is in fact a sign of pathology.
Specific patterns: presence of temporal theta, also known as temporal sawtooth. An example of a temporal sawtooth pattern is shown in figure A.4A. A temporal sawtooth pattern consists of a series of sawtooth-shaped increases in amplitude with frequencies in the range of 4.5 to 6Hz. As already explained by its name, these patterns are typically observed in temporal areas.

29-33 Weeks CA

States: initially one undifferentiated state. At the end of the period the differentiation to one state of sleep and one state of wakefulness begins.
Background: tracé discontinu. Most burst activity appears asynchronous. Burst periods become longer and interburst intervals shorter.

Specific patterns: maximal presence of temporal theta at 29-31 weeks CA [3]. Delta brushes also start to appear and have their maximal abundance at 32-34 weeks CA. An example of a delta brush is shown in figure A.4B. A delta brush consists of a theta wave of about 8Hz superposed on a much slower delta wave with an amplitude in the range of 50 to 300 μV [8]. At 29 weeks CA delta brushes appear mostly in the central areas of the brain. Later on their presence is highest in the temporal and occipital areas.

34-37 Weeks CA

States: at the beginning two states exist, one sleep state and one state of wakefulness. Around 35 weeks the sleep state differentiates further to a state of quiet sleep and a state of active sleep. At 35 weeks quiet sleep occupies 40% of the total time spent by sleeping.
Background: tracé continu for the state of wakefulness and later on also for the state of active sleep. A background pattern is defined as tracé continu whenever the amplitude reaches values above $20\mu V$ and there is no clear division possible in periods of high activity and low activity. Tracé discontinu is still observed for the quiet sleep state. The length of bursts increases and the length of IBIs decreases again. Activity is partly synchronous.
Specific patterns: the temporal sawtooth pattern has almost disappeared, only in active sleep sawtooths are still observed occasionally. The abundance of delta brushes is maximal at the beginning of this age interval. The number of delta brushes slowly decreases during the further development of the brain. Two new patterns arise in the frontal areas during this period. At 34 weeks CA encoches frontales are detectable and at 35 weeks CA anterior slow dysrhythmia appears during active sleep. An example of these two patterns can be found in figure A.5A and B respectively. Encoches frontales, also known as ripples of prematurity or frontal sharp transients, appear most often between 36 and 38 weeks CA. Encoches frontales are observed as diphasic sharp waves with a voltage of 50-200 μV and a duration of 0.5-0.75s. Their frequency is variable [3]. Anterior slow dysrhythmia consists of mono- or polyphasic delta activity with frequencies of 1 to 3 Hz and amplitudes of 50 to 100 μV. The maximal amount of anterior slow dysrhythmia is observed at 36 to 37 weeks CA in active sleep [3].

38-42 Weeks CA

States: three states can be distinguished: active sleep, quiet sleep and wakefulness. The percentage of sleep occupied by both quiet and active sleep states is 50% at fullterm age.
Background: Tracé continu in active sleep and wakefulness. Tracé alternant during quiet sleep. Tracé alternant is a background pattern that is an intermediate of tracé discontinu and the continuous pattern. It has periods of predominantly slow activity with large amplitudes(1-3Hz and 50-100μV) and periods of faster activity(4-7Hz) with a lower voltage [3]. The background's amplitude during the latter periods is however larger than the $20\mu V$ of the IBIs of tracé discontinu. Only minor asynchronies are present.
Specific patterns: temporal sawtooth, and delta brushes are only sporadically observed in this stadium. The number of encoches frontales and anterior slow dysrhythmia also decreases during this period.

Summary

In short the EEG signal matures from a discontinuous signal to a continuous signal, the length of burst periods increases, the IBIs shorten, the amplitude of the burst periods decreases and the amplitude of the IBIs increases. This change from tracé discontinu to tracé continu is first observed in the 'active' states of wakefulness and active sleep. Next to this, EEG activity becomes more symmetrically and synchronous as the brain develops, except for a small period of hypersynchronicity around 27 weeks of CA.

2.3.3 The abnormal EEG of the full-term newborn

In the previous paragraph the normal 'maturation' of the EEG has been described. In general an EEG signal is defined as abnormal when it has properties that are not expected for a normal EEG of the specific CA and state. In the next part the abnormal EEG signal for the full-term newborn will be discussed. The reasons for focussing on the full-term newborn are presented first.

The variety of signals that can be interpreted as being normal, increases as CA decreases. This has two main reasons. The first is, that the interindividual rate of brain development in earlier periods differs already a lot for healthy infants, not to mention the variability observed for pathological infants. Of course this variability is reflected in the EEG signal. This has led to the acceptation of a very large scala of EEG properties as being normal at these ages. It is really hard to find an EEG signal at these ages, that can be interpreted as being abnormal without doubting. Secondly, the brain is still highly moldable at these ages. This means that whenever certain parts of the brain are damaged and lose their ability to perform specific functions, other parts of the brain are capable of gaining the ability to perform these functions either fully or partially. In this way the brain regains certain abilities in spite of its damage. This regaining ability decreases as age increases. A prognosis based on a single EEG recording in these early stadia is therefore of very little significance. This causes the interpretation of an EEG at early ages to be really though.
The fact that the brain has become much more stabilized at full-term age and the resulting better capability of distinguishing between an abnormal and normal EEG registration, has led to the choice to focus on full-term newborns. It is expected that if it is not possible to find a relation between a quantitatively described EEG of a full-term newborn and the clinical outcome of the same child at a later age, that it is highly unlikely that such a relation does exist for an EEG registration recorded at an earlier age.
The degree of abnormality of the qualitative EEG is usually related to the type of background present in the EEG. Pathological background patterns at fullterm age are, in order of decreasing severity of prognosis: iso-electric background, low voltage background, burst-suppression background and a persistent tracé alternant background [12]. The definition of an iso-electric background is a background signal that doesn't have any activity above $5\mu V$ [12]. A low voltage background is defined as a background signal with amplitudes not rising above $20\mu V$. A burst-suppression background is equal to the non pathological background pattern tracé discontinu, which is observed at earlier ages. The final background pattern, persistent tracé alternant, is a tracé alternant background, which persists in active sleep and wakefulness. This is also considered to be a sign of pathology.
Next to these pathological background patterns, which the are illustrated in figures B.1, B.2 and B.3, the occurrence of specific abnormal patterns also contributes to the degree of abnormality. Abnormal patterns mentioned in literature are positive rolandic sharp waves (PRSWs) and epileptiform seizures. An example of a PRSW is observable in figure B.4. In general, the appearance of PRSWs only strengthens the conclusions made on a basis of the background pattern. The appearance of this pattern on a normal background is of no prognostic significance.
Finally, it is possible that patterns normally seen for earlier conceptional ages are observed in the EEG registration at full-term age, which is usually interrelated to a lag in maturation of the brain. Whenever the patterns correspond to a lag in maturation of more than 2 weeks this is also considered to be a sign of abnormality.

2.3.4 Medication

When interpreting a full-term EEG signal caution should be taken when the neonate is receiving medication. This is almost always the case. It is known, that some drugs have influence on the EEG recording. The knowledge in this field is however scarce [16]. A number of drugs are suspicious of increasing discontinuity and therefore often cause burst-suppression alike patterns to arise. Phenobarbital, a medicine used to suppress electrographical seizures, is one of these [3]. Morphine, used to improve assisted ventilation for respiratory or systemic problems or to provide analgesia has similar effects as phenobarbital, is another one [18]. Other medications with possible similar effects are benzodiazepines, propofol, pentothal, and sufentanil [14]. The dose of medication is also expected to play a role.

2.3.5 Artifacts

Another pitfall when interpreting EEG signals is to mistake artifactitious electrical activity from other sources for EEG activity. A number of artifacts present in EEG registrations are summarized in the table in figure 2.3.
To prevent these kind of pitfalls a number of the other electrophysiological signals summed in the preceding table are measured simultaneously with the EEG channels. In this way the neurophysiologist can easily

Artifact	Source
50Hz	Electromechanical devices
High frequent activity	Muscle movement (EMG)
ECG activity	Depolarization and repolarization of the heart (ECG)
Baseline drift	Sweating
Repetitive periods of single frequent activity	IVAC / infusion pump
Signal loss	Cable disconnection, malfunctioning electrode
Transient activity in frontal derivations	Eye dipole movement (EOG)
Pulse artifact	Electrode movement caused by pulsating arteries
EMG artifacts	Hick-ups, Sucking, Crying

Table 2.3: *Artifacts in EEG registrations and their sources*

recognize activity which occurs simultaneously in EEG channels and for instance in an EMG channel (electromyogram) and conclude that the electrical activity measured in the EEG channels is in fact originating from muscle movement. Another means to recognize for instance muscle artifacts is the recording of a video during measurement. The synchronicity of movements with EEG activity can then be used to detect movements artifacts. Of course, the recording of a video also provides extra information about the clinical state of the newborn.

2.4 Analysis techniques

As described before, the frequency content of the EEG signals is often analyzed to obtain additional information. To transform a signal from the time domain to the frequency domain, the Fourier transform is usually applied.

2.4.1 Fourier transform

The Fourier transform of a continuous infinite signal $s(t)$ is defined as

$$S(f) = \mathcal{F}[s(t)](f) = \int_{-\infty}^{\infty} s(t) \exp^{-2\pi i f t}\, dt, \tag{2.1}$$

where f is the frequency. For a finite signal $s(t)$ with length T equation 2.1 becomes

$$S(f) = \int_{0}^{T} s(t) \exp^{-2\pi i f t}\, dt. \tag{2.2}$$

In experiments the signal is not measured continuously, but sampled at a sample frequency, f_s. Therefore a discrete version of equation 2.2 is used, the DFT:

$$S(f_n) \approx S_n \Delta t = S_n \frac{T}{N} = \frac{T}{N} \sum_{k=0}^{N-1} s_k \exp^{\frac{-2\pi i k n}{N}},\ n = -\frac{N}{2} + 1, ..., \frac{N}{2},\ k = 0, 1, ..., N-1. \tag{2.3}$$

Here N is the total number of samples, s_k the signal at time $k\Delta t$, with $\Delta t = 1/f_s$,and $S(f_n)$ the complex amplitude for a frequency interval $f_n = n\Delta f$, with $\Delta f = 1/T$. These frequency intervals are also called frequency bins. The frequency range these bins describe is

$$-\frac{f_s}{2} < f_n \leq \frac{f_s}{2}, \tag{2.4}$$

of which only the positive frequencies are of physical value. Due to the complex shape of equation 2.3 the spectral content in the negative frequency bins is a mirrored copy of the spectral content in the frequency

bins from 0 to $\frac{f_s}{2}$. Therefore the energy, U, of the signal can be calculated by multiplication of the energy content in the 'single-sided' spectrum by 2

$$U = 2\int_0^{\frac{f_s}{2}} |S(f_n)|^2 df \approx \Delta f \sum_{n=0}^{N-1} |\frac{T}{N} S_n|^2 = \frac{T}{N^2} \sum_{n=0}^{N-1} |S_n|^2. \tag{2.5}$$

The average power, P, is then calculated by

$$P = \frac{U}{T}. \tag{2.6}$$

To prevent aliasing when performing a DFT the Nyquist criterion must be met. The Nyquist criterion requires a signal to be sampled at least at two times the highest frequency component it contains.

2.4.2 Parseval theorem

Of course the energy of a signal $s(t)$ can also be calculated in the time domain

$$U = \int_0^T |s(t)|^2 dt \approx \frac{T}{N} \sum_{k=0}^{N-1} |s_k|^2. \tag{2.7}$$

By combining equations 2.5 and 2.7 the Parseval Theorem is found, which states that energy is conserved in the Fourier Transform

$$\sum_{k=0}^{N-1} |s_k|^2 = 1/N \sum_{n=0}^{N-1} |S_n|^2. \tag{2.8}$$

2.4.3 Spectral leakage

The complex shape of a discrete Fourier transform causes signals of finite length to be considered as if they were infinitely long with a periodicity of T. In case of the transform is carried out for a non-periodic signal this causes discontinuities to appear at the start of every new period, which is illustrated in figure 2.9.

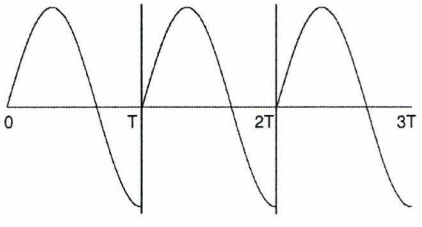

Figure 2.9: *Illustration of the discontinuities that arise at the edges of each period, when periodically expanding a signal with finite length T, during a Fourier transform*

These discontinuities in the time domain are responsible for spectral leakage in the frequency domain. Spectral leakage is the displacement of energy from a given frequency to other frequency bins in a spectrum. Spectral leakage is explained by regarding a finite signal as a truncation of an infinite signal by a rectangular window. A truncation by a rectangular window is in fact the product of a rectangular window and the infinite signal. The product of two signals in the time domain, is equal to the inverse Fourier transform of the convolution of the two signals in the frequency domain:

$$s(t)w(t) = \mathcal{F}^{-1}[\mathcal{F}(s(t)) * \mathcal{F}(w(t))]. \tag{2.9}$$

The Fourier transform of a rectangular window is a sinc function. The side lobes of this sinc function are responsible for the leakage of energy to other bins as illustrated in figure 2.10.

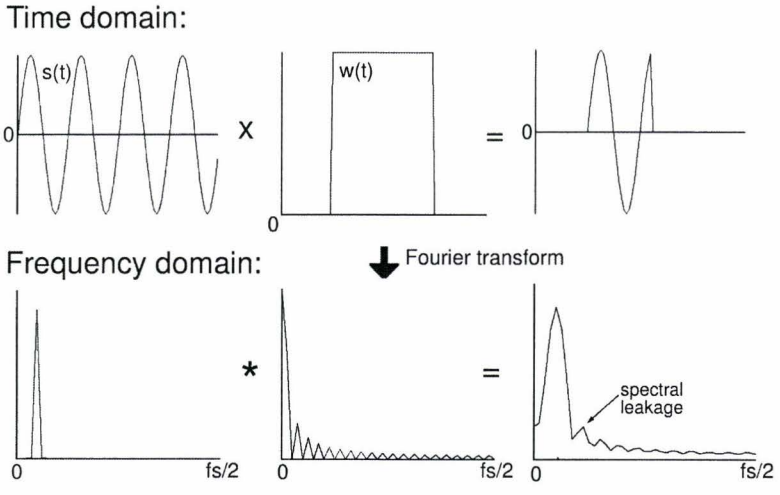

Figure 2.10: *Illustrative example of spectral leakage appearing whenever a signal is truncated with a rectangular filter*

To reduce spectral leakage a Hanning filter is applied to the signal. This Hanning window smooths out the ends of the measured signal in such a way, that start and ending have a zero slope and a value of zero, which removes the discontinuities at the edges. The Hanning window and its Fourier transform are shown in figure 2.11.

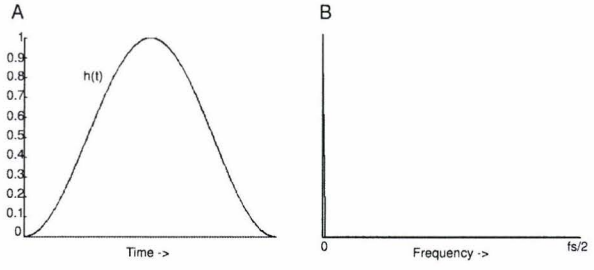

Figure 2.11: *The Hanning window and its Fourier transform*

It should be noticed that the Hanning filter is responsible for a reduction of the signal's spectral power. Therefore a correction of this power has to be carried out, which implies the division of the power spectrum by the average power of the Hanning window

$$P_{Hanning} = \frac{3}{8}\frac{N-1}{N}. \tag{2.10}$$

2.4.4 Short-time Fourier transform

The frequency composition of most biomedical signals is changing over time, this is also the case for the EEG signal. In order to follow the spectral changes in time, the Fourier transform is carried out for separate parts of the signal, the Short-time Fourier transform:

$$STFT(t,f) = \int s(\tau)h(\tau - t)e^{2\pi i f \tau} d\tau. \tag{2.11}$$

Here $h(t)$ is a window function with a windowlength equal to τ. The window moves along the signal. At each sample point the signal content in the window, which has a length of τ, is filtered with the window function and its spectrum is calculated. The spectrum calculated has a frequency resolution of $\Delta f = \frac{1}{\tau}$. This relation of τ and Δf leads to a trade-off in time and frequency resolution. To follow fast changes in frequency content $\tau = \Delta t$ has to be as small as possible, leading to a deterioration of frequency resolution.

2.5 Filters

To remove specific frequency components of a signal, like the 50Hz interference caused by electromechanical devices, a digital filter is usually applied. The characteristics of a filter are defined by its transfer function. The transfer function describes the relation between the unfiltered input signal and the filtered output signal. Each of the frequency components present in the unfiltered signal return in the filtered signal as a frequency component of the same frequency, however with a phase shift and a magnification of amplitude. This implies that for a sinusoidal input signal

$$x(t) = A\cos(\omega t), \tag{2.12}$$

the filtered output signal $y(t)$ is equal to

$$y(t) = AM\cos(\omega t + \phi). \tag{2.13}$$

Here M represents the magnification factor, and ϕ represents the phase shift. Of course this phase shift can be zero and the magnification factor can be one, which means that the frequency component is exactly the same before and after filtering. From the transfer function the frequency response of a filter can be derived. The frequency response describes the changes in magnification factor and phase shift of the output signal with respect to the input signal for each frequency. By altering the frequency response it is possible to design filters with special properties. In general four types of filters are known: low-pass filters, high-pass filters, band-pass filters and band-stop filters. A low-pass filter passes the lower frequencies of a spectrum and attenuates the higher frequencies. A high-pass filter functions vice versa. A band-pass filter attenuates all frequencies, except for the frequencies in a defined frequency band. A band-stop filter only attenuates frequencies in a specific frequency band. The bands of frequencies, that are attenuated or passed, are referred to as stopband and passband respectively. The division in stopband and passband is made on basis of the cut-off frequency. The cut-off frequency is defined as the frequency at which the frequency response is equal to $2^{-\frac{1}{2}}$.
Proper analysis of an EEG signal is unimaginable without the application of a number of filters. The filters applied during this project are all Butterworth filters. The reason for choosing Butterworth filters is, that these filters have an optimally flat passband. This means that all frequencies in the passband are passed with a same magnification factor. The magnification factor of the frequency response of a Butterworth low-pass filter is given by

$$|H(\omega)| = \frac{1}{\sqrt{1 + (\frac{\omega}{\omega_c})^{2n}}}, \tag{2.14}$$

where n is the order of the filter, ω is the frequency, and ω_c corresponds to the cut-off frequency. In figure 2.12 the attenuation of a signal filtered with a fourth order Butterworth low-pass filter with a cut-off frequency at 75Hz is shown. The attenuation is shown as a function of the frequency, which is normalized with respect to half the sampling frequency $f_s = 256Hz$. The normalized cut-off frequency is $0.59\pi rad/sample$. This filter is applied to remove high frequency content, which is not of EEG origin, like the harmonics of the 50Hz powerline signal. A downside to Butterworth filters is, that the roll-off steepness is rather low compared to other filters like a Chebyshev 1 filter. This means that the amplitudes of the frequency components in the pass-band are relatively less attenuated than they would had been after filtering with a Chebyshev 1 filter.

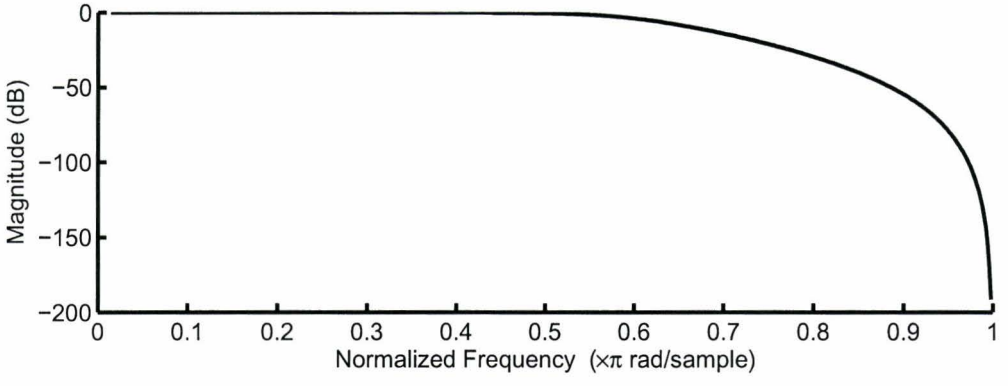

Figure 2.12: *The attenuation of a signal filtered with a fourth order Butterworth low-pass filter with a cut-off frequency at* $0.59\pi rad/sample$ *plotted as function of the normalized frequency.*

As mentioned before, filtering can also impose a frequency shift to frequency components. Such phase shifts are not wished when analyzing an EEG signal. To correct for phase shifts the signal is filtered once in forwards direction, which imposes a phase shift of $\phi(\omega)$, and once in backwards direction, which cancels out the previous phase shift by imposing a phase shift of $-\phi(\omega)$.

Chapter 3

Experimental setup

3.1 Data acquisition

3.1.1 System

The data acquisition system used for the measurement of the neonatal EEG in the Máxima Medical Center in Veldhoven is the NicoletOne Monitor with Video and a C32 amplifier. A schematic representation and a picture of this system is shown in figure 3.1. The system is a PC based digital EEG system. The PC is integrated in a touchscreen monitor as a PanelPC.

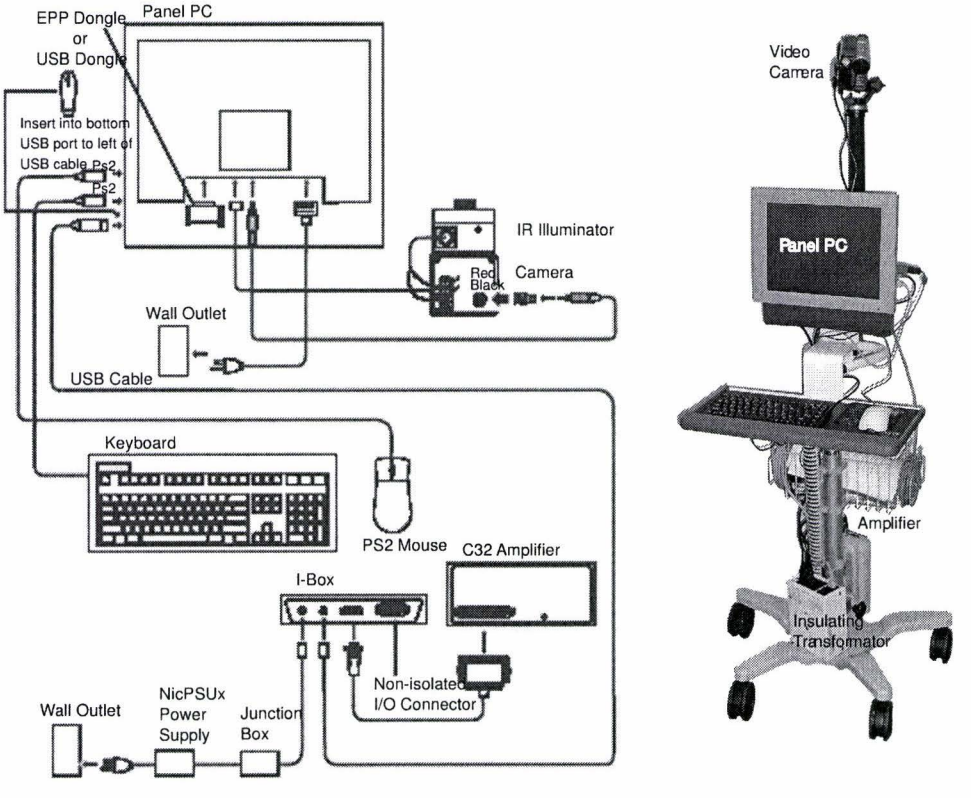

Figure 3.1: *Schematic presentation and a picture of the data acquisition system used in Veldhoven*

The EEG signals are digitized with a 22-bit AD converter at a sampling rate of 512 Hz in the Máxima Medical Center in Veldhoven. The EOG and respiration signals are sampled at a lower frequency of 16Hz. Data is saved in a file format that has been especially developed for the NicoletOne Monitoring systems. Data can be exported to the edf file format. The edf format, or European data format, is a universal file format in which polygraphic eeg recordings can be saved. Because the edf format does not support information about annotations, an extended version of the edf format, the edf+ format has been developed. A detailed description of the edf/edf+ format is given in Appendix C.
The department of Neurophysiology of the UMC St.Radboud in Nijmegen makes use of an earlier version of the system also with 32 channels available for recording. Here, all signals are digitized at 256Hz, except for the respiration signal, which is also sampled at the lower sampling frequency of 16Hz.

3.1.2 Electrodes

Measurements in Nijmegen and Veldhoven are performed differently. First the procedure of measurement in Veldhoven is decribed.
In Veldhoven a full EEG is recorded, which means that all electrodes shown in figure 2.8 are measured. The electrodes used are AgAgCl-cup electrodes. Each electrode is held in place by collodium and a gauze. Once the electrodes are attached to the scalp, a paste of KNaCl is inserted between the cup of the electrode and the scalp of the neonate. This paste, which is insensitive to contamination, serves as a conductor for the signal from the skin to the electrode by forming a connection between the silver of the electrode and the scalp. This connection also causes the electrode impedance to be high for the environment. Electrode impedances are held below 5kΩ during the recordings.
In Nijmegen registrations are performed with only 9 electrodes: Fp1, Fp2, T3, C3, Cz, C4, T4, O1, and O2. This configuration is known as 'small electrode', or 'baby' configuration. Before the attachment of the electrodes, the skin is cleaned with 'Nuprep EEG and ECG skin prepping gel'. Each electrode is then attached with an adhesive 'Fixomul strech' gauze. To improve the conduction a conductive paste 'Ten20 Conductive Paste' is inserted between the electrode and the skin. The electrodes used in Nijmegen are also cup electrodes. They are made of tin, which is also insensitive to contamination. Electrode impedances are also held below 5kΩ during the recordings.

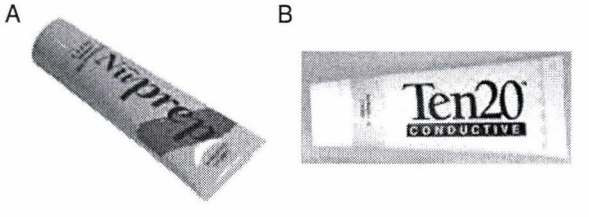

Figure 3.2: *Pictures of A: the cleaning gel, and B: the conductive paste used in Nijmegen*

In both Veldhoven and Nijmegen polygraphic recordings are performed. Therefore additional sensors for the recording of activity of other physiological sources are placed. Usually sensors for the measurement of ECG, chin-EMG, abdomen movements, respiration, and horizontal, vertical and diagonal EOG are placed.

3.2 Experiments

All but one EEG registration, that are used for the analysis, have been recorded in the UMC in Nijmegen. Therefore only the channels corresponding to the baby configuration have been taken into consideration for the analysis of the EEG registration performed in Veldhoven.

3.2.1 Background classification

As mentioned before, the interpretation of an EEG signal is carried out in steps, starting with the determination of CA and state. During the next step the determination of the background pattern plays an important role. It has been shown, that the background pattern of the EEG contains the most reliable information about the clinical development of a neonate [12, 17]. A first step towards the project's goal, determining the degree of functioning of the brain, based on EEG recordings not long after birth, is to recognize, and classify, background patterns by means of an algorithm. Such an algorithm has been developed during this project and is described in the next chapter. To validate the functioning of the algorithm, 10 signals with a total duration of 4 hours have been analyzed by the algorithm. The outcome of the general background classification generated by the algorithm has been verified by an expert on neurophysiology from Veldhoven.

3.2.2 Burst detection

Based on background patterns alone, only superficial statements can be made about the prognosis of full-term newborns. Newborns with a healthy prognosis are distinguishable from newborns with a very grave prognosis, in between is a large group of newborns with an unclear prognosis. The background pattern, most often observed for this last group, is a burst-suppression background. It is expected that a separate analysis of bursts and interburst intervals(IBIs) will make a further subclassification of prognosis possible [13, 2]. To analyze bursts and IBIs, the bursts first have to be separated from the IBIs. An algorithm has been developed, that is dedicated to the separation of bursts and interburst intervals. The algorithm is described in paragraph 4.2.5. For the validation of the algorithm the expert from Nijmegen has been asked to annotate burst, artifact, and other EEG activity for 8 burst-suppression signals of asphyxiated full-term newborns with a total signal length of 3 hours and 40 minutes. The annotated burstperiods are compared to the burst periods detected by the algorithm.

3.2.3 Burst and IBI parameters

It is expected that a separate analysis of burst and IBI might provide the ability to determine the life chances of a newborn with an otherwise unclear prognosis. To this end burst parameters and IBI parameters are defined and calculated. The definitions of these parameters are presented in the final paragraph of the next chapter. To be able to find a possible relationship between these parameters and a specific prognosis, it is necessary that the variables correctly quantify the signal. In order to investigate whether the quantification is performed correctly, 5 burst-suppression EEG recordings are divided into parts of 10 minutes. Next, for each recording segment of 10 minutes all parameters are calculated and the intersegmental variation of each parameter per recording is determined. Is this variation small, than the parameter is representative for the entire recording and the quantification is considered to be correctly. Next to the intersegmental variation, also the variation of the parameters over the various areas of the head will be investigated.

Chapter 4

Algorithm

4.1 Global functioning

A flowchart of the main steps performed by the algorithm is shown in figure 4.1A. All of the steps have been implemented in a graphical user interface.
During the first step a binary datafile in edf format is read and decoded.
As the flowchart shows, pre-analysis takes place next. During this pre-analysis general information about the signal's background pattern is gathered and 'burstprobability vectors' are calculated. The function and determination of these vectors and the rest of the pre-analysis is discussed in detail in the next paragraph.
After the pre-analysis, the channels of interest for further analysis are selected and their corresponding signals are derived from the raw signals. For instance if the raw signal is known for the channels C3-O1 and C4-O2, and the channel chosen for analysis is C3-C4, then the signal of the new channel is calculated by subtraction of the raw data corresponding to C4-O2 from the raw data corresponding to C3-O1. In some cases two subtractions are necessary for the calculation of the data of the new channel. This is for instance the case if the raw signal is known for the channels C3-O1, C4-O2 and O2-O1, and the channel C3-C4 is chosen for analysis. The raw data for the new channel C3-C4 is obtained by subtracting the data of O2-O1 from the data of C4-O2 and then subtracting the signal resulting from the first subtraction from the data of C3-O1.
During the next step at least three filters are applied to the derived signals: a high-pass filter with a cut-off frequency of 0.5Hz, a low-pass filter with a cut-off frequency of 75Hz, and a notch filter at 50Hz. The high-pass filter is applied to remove the artifactitious baseline wander caused by electrode movement and sweating of the patient. The low-pass filter is applied to attenuate the high frequency content of the signal, that does not correspond to EEG activity. The notch filter is used to effectively remove the 50Hz interference signal generated by electrical devices. In addition a notch filter with cut-off frequencies around 10Hz is automatically applied, whenever a 9.9Hz interference signal is detected. This 9.9Hz interference signal arises whenever the neonate receives high frequent oscillation (HFO) ventilation during the EEG registration. The 9.9Hz interference signal is detected on basis of a STFT with windows of 60 seconds. Whenever most power resides in the bin corresponding to a frequency of 9.9Hz for at least half of the EEG channels this hfo filter is activated. All of the mentioned filters are 4th order butterworth filters.
Step 5 involves the detection of movement artifacts for the signals belonging to the channels of interest.
During step 6, a 4th order low-pass butterworth filter with a cut-off frequency at 32Hz is applied to attenuate frequency content in frequency bins higher than 30Hz. In this way mainly frequency content in the EEG range remains, which then is analyzed further. This filter is not applied earlier, because movement artifacts are often expressing themselves at frequencies of 30Hz and more.
The analysis of the filtered signal starts with the classification of the background pattern of each of the chosen channels. Whenever the background classification of a channel fulfills certain later described rules, in addition a burst detection procedure is performed.
During step 8, bursts that have been detected with a certain probability are selected. This principle is discussed in depth in paragraph 4.3.

The last step, discussed in paragraph 4.4, consists of the analysis of the signal in the chosen channels. The values of the burst and IBI parameters resulting from this analysis quantify the signal.

4.2 Pre-analysis

As mentioned in the last paragraph, the pre-analysis serves to obtain general information about the signal's background pattern and to calculate a number of 'burstprobability' matrices. The pre-analysis is carried out in a special way. It is performed independent of the channels chosen for analysis and secondly it takes the possible existence of a single bad electrode during the recording into account. This is achieved in a number of steps. These steps are visualized in the flowchart of figure 4.1B.

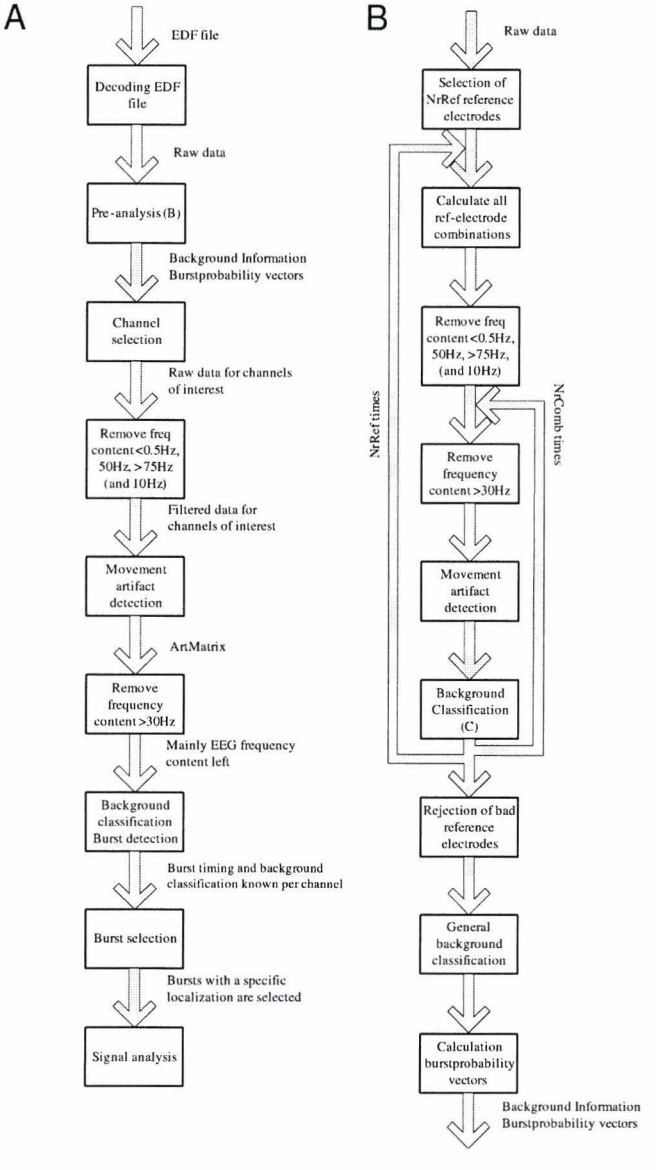

Figure 4.1: *A: Flowchart of the main parts of the algorithm, B:Flowchart of the pre-analysis*

First, a number of $NrRef$ artificial reference electrodes is chosen. The reference electrodes used for this project are: Cz, T4 and T3. These electrodes are chosen for two reasons: they provide information about a large area of the brain and they are relatively free of electrical activity caused by artifacts. The next step involves the calculation of all EEG derivations that can be constructed with each reference electrode. The $NrComb$ signals corresponding to the combinations per reference electrode are then filtered with the filters described for step 3 in the preceding paragraph. Next, each of these channels is separately analyzed. This analysis, that consists of three parts, steps 4 to 6 in the flowchart of figure 4.1B, is discussed in the next two subparagraphs. After the rejection of possible bad reference electrodes, a procedure described in subparagraph 4.2.3, general information about the background classification is obtained and the so-called burstprobability vectors are calculated. In subparagraph 4.2.6 the term 'burstprobability vector' is explained and the calculation of the vectors is described.

4.2.1 Detection of movement artifacts

In figure 4.2 an EEG signal in the time domain and its corresponding spectrogram are presented. In this signal two movement artifacts are present. As can be observed in the time domain representation, these artifacts are easily mistaken for burst activity. In frequency domain however, movement artifacts are often better distinguished from burst activity, because movement artifacts often contain more high frequent components.

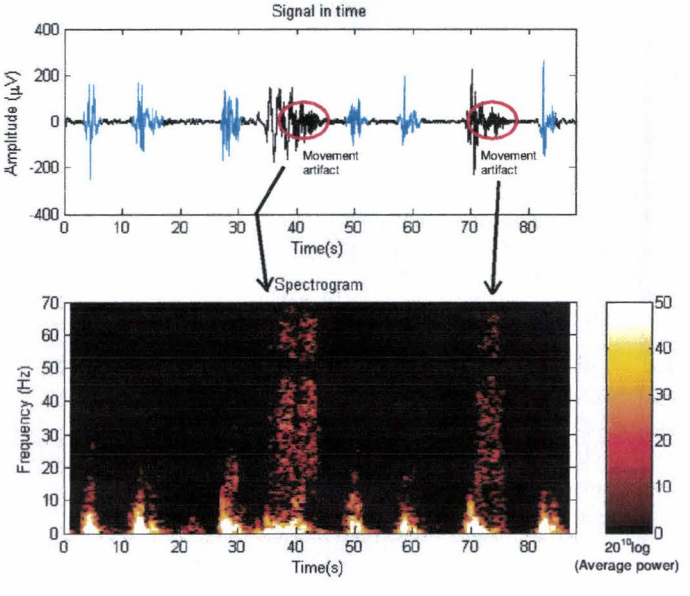

Figure 4.2: *A signal and its corresponding spectrogram showing the high frequent components of movement artifacts. Burst activity is shown in blue.*

The detection of movement artifacts is based on this knowledge. Most movement artifacts are characterized by a high frequency component ranging from 25Hz up to higher frequencies. A movement artifact is detected whenever the average power residing in frequencies from 25Hz upwards calculated over 0.25 seconds of the signal crosses a threshold of $150\mu V.^2$. This threshold has been determined empirically.
After the application of a high-pass 4th order butterworth filter with a cut-off frequency at 23Hz, the average power residing in frequencies from approximately 25Hz upwards is calculated from the signal in the time domain according to equations 2.7 and 2.6. The filter is applied to make sure that frequency components of 25Hz and higher are passed without attenuation and that frequencies below 25Hz are attenuated or even filtered out. The average power is calculated per sample point over the next 0.25 seconds. This calculation

is performed in a fast way by first squaring the original signal and then applying a moving average window filter with the aforementioned windowlength.
All samples with an average power value above the threshold of $150\mu V^2$ are now labeled as being artifactitious. However, because the average power in artifacts at the onset of the artifact and at the ending of the artifact is below the threshold of $150\mu V^2$, a little error will be made in the calculation of the precise onset and ending of these artifacts, as illustrated in figure 4.3. To reduce this error, the minimum in average power before and after these roughly determined start and endpoints of each artifactitious part are determined. The newly determined precise onset of the artifact is however still not correct. It also has to be corrected for the hysteresis effect caused by the windowing, illustrated as 'shift' in figure 4.3.

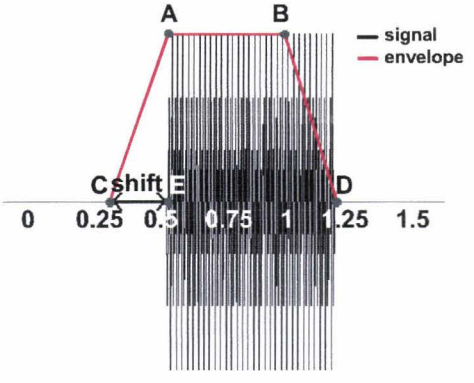

Figure 4.3: *The determination of movement artifacts A:Roughly determined artifact onset, and B: ending. C:Precise artifact onset defined as the previous minimum in the average power without taking shift caused by windowing in account. D:Precise artifact ending defined as the next minimum in the average power. E:Precise artifact onset after correction for the shift caused by windowing.*

The parts of the signal that are located between the onsets and their corresponding endings and that are therefore considered artifactitious, are saved in a matrix called $ArtMatrix$. Each column in the matrix contains movement artifact information of a specific channel. Each row represents a sample position. Whenever an artifact is detected in a specific channel for a number of samples the elements of the column representing the channel, which correspond to the samples, receive the value 1. The elements of the matrix that are representing non-artifactitious parts of the signal receive the value 0:

$$ArtMatrix(i, ch) = 1, \text{ for movement artifacts} \quad (4.1)$$
$$ArtMatrix(i, ch) = 0, \text{ otherwise} \quad (4.2)$$

where i is the sample and ch is the number of the ref-electrode channel.

4.2.2 Background classification

During this part of the pre-analysis, the background pattern of the signal of each ref-electrode combination is classified. There are five possible classifications for the background pattern of a channel at full-term age: iso-electric, low voltage, burst-suppression, (persistent) tracé alternant, and tracé continu in decreasing degree of severity of the prognosis. A sixth classification with the label 'undefined' is added to these five classifications. A signal is classified as 'undefined' whenever the normal background classification is considered to be unreliable. A flowchart for the background classification algorithm of a single signal is shown in figure 4.4.

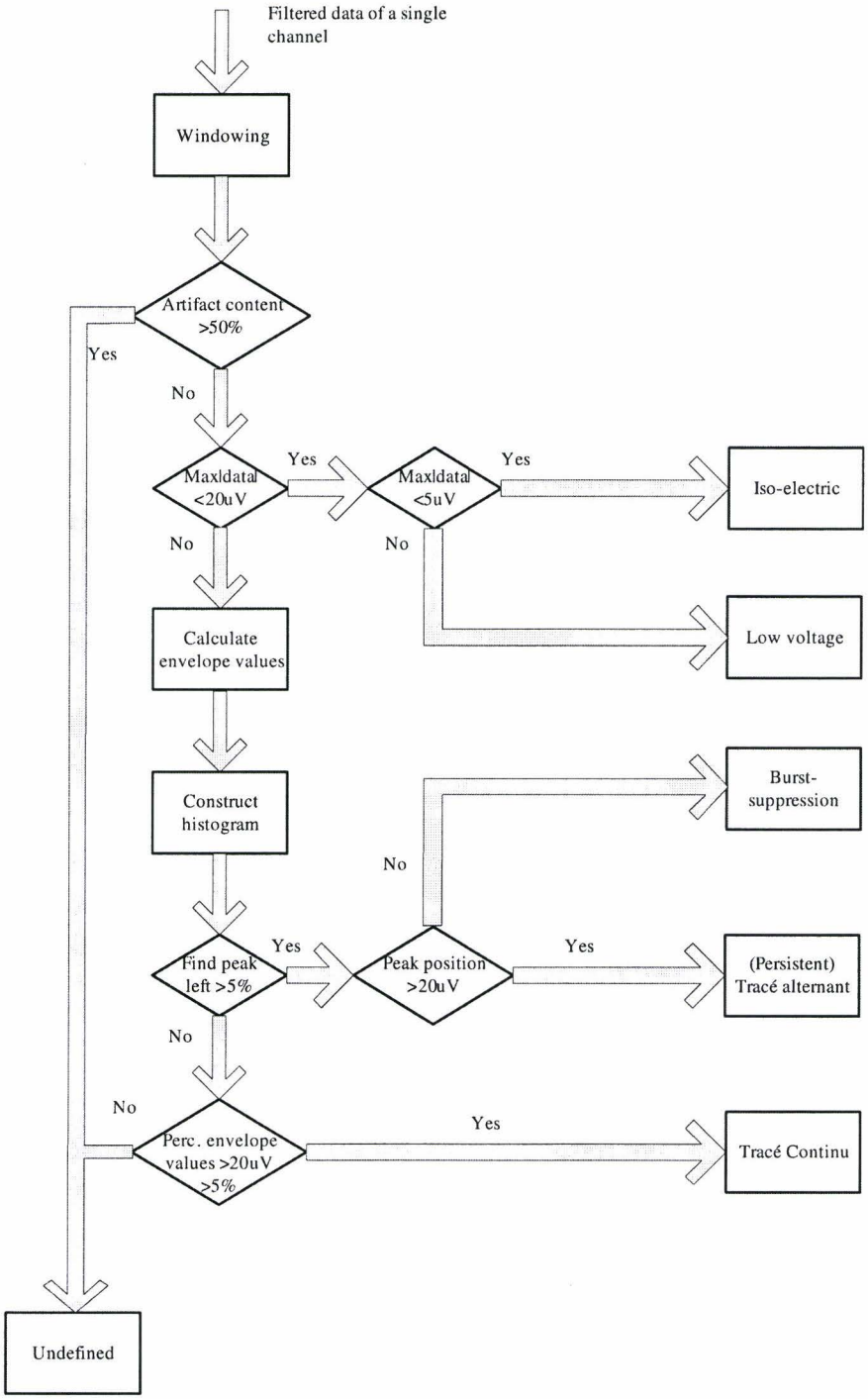

Figure 4.4: *Flowchart of the background classification procedure*

As can be observed in this flowchart, first the signal is windowed with half overlapping windows with a windowlength of 20 seconds. This windowlength is chosen for two reasons. The first reason is related

to the fact that bursts are usually found to last no more than ten seconds [15]. This implies that a certain amount of IBI is always present in each window, provided that the signal is of the burst-suppression type. This is necessary for a correct detection of bursts, which is made clear in the next subparagraph. The second reason is also related to burst detection. The windowlength is not allowed to be much larger than the maximal burstlength, because of the necessary frequent update of the threshold value above which bursts are detected. This will also become clear from the next subparagraph.
Next, calculations for each windowed part of a signal are performed. First, the percentage of artifacts in the window is determined from the corresponding elements of the matrix $ArtMatrix$. Whenever this percentage is larger than 50% , which is equal to 10 seconds of artifactitious signal, the background classification procedure is considered to be unreliable, and thus the background pattern of the window is classified as 'undefined'. In all other cases the background classification procedure is continued.
The classification is continued with an analysis of different representations of the signal in time. These representations and an example signal are shown in figure 4.5.

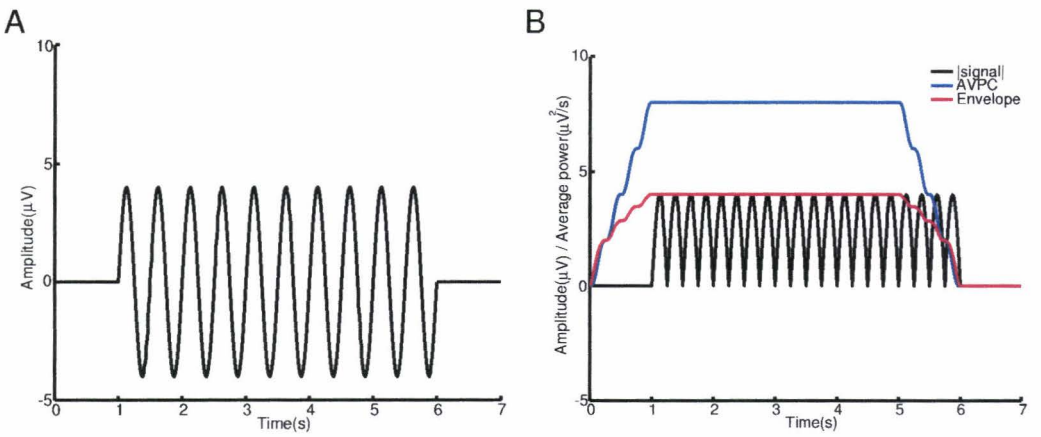

Figure 4.5: *A:Signal, B:Different representations of the signal in time: the absolute signal, envelope signal and average power content signal(APCV).*

First, the maximum value of the absolute signal, the black line in figure 4.5B, is calculated. A signal with a maximum absolute value below $5\mu V$ is classified as being iso-electric. In case a maximum absolute value of less than $20\mu V$, but larger than $5\mu V$ is detected, the background is defined as a low voltage background. Both classifications are performed on basis of the definitions given in paragraph 2.3.2.
The signals with a maximum absolute value of more than $20\mu V$ remain to be classified. The background classification of these signals is carried out by analysis of the envelope signal, which is illustrated in figure 4.5B. To obtain the envelope values, first the average power content values have to be calculated. These values represent the average power contained in a second of the signal. These APCVs are calculated with the same moving average window technique as described in the preceding subparagraph. The windowlength is however now chosen to be one second, because the lowest frequency component present in the filtered squared signal is 1Hz, which has a period of 1.0s. The envelope values are calculated from the APCVs by

$$Envelope = \sqrt{2APCV}. \tag{4.3}$$

The envelope values corresponding to a second of the signal in which movement artifacts occurred are rejected. The remaining envelope values, which are not influenced by movement artifacts, are then plotted in a histogram. The histogram is divided in 100 equally spaced bins. The first bin corresponds to the lowest envelope value, the final bin corresponds to the largest envelope value. Examples of resulting histograms for burst-suppression, tracé alternant and tracé continu are shown in figure 4.6. On the vertical axis the ratio of envelope values in a specific bin and the total number of envelope values is displayed.
As can be observed, the histogram of the tracé continu background is characterized by a more or less equal distribution of envelope values over all bins. The shape of the histogram of the burst-suppression

background, and also of the tracé alternant background, is more peaked. The envelope values are mainly distributed over a small number of bins. This peaked shape is caused by the alternating appearance of periods with high and low amplitude. The algorithm makes use of this difference in shape to distinguish tracé continu from the other two backgrounds. It searches for bins in the first half of the histogram that contain more than 5% of all envelope values. If such a bin is not existing, which is usually observed for tracé continu, the background is classified as tracé continu, unless the percentage of envelope values in bins above $20\mu V$ is less than 5% of the total number of envelope values. If this is the case, the background classification procedure is again assumed to be unreliable and the background signal is classified as undefined.

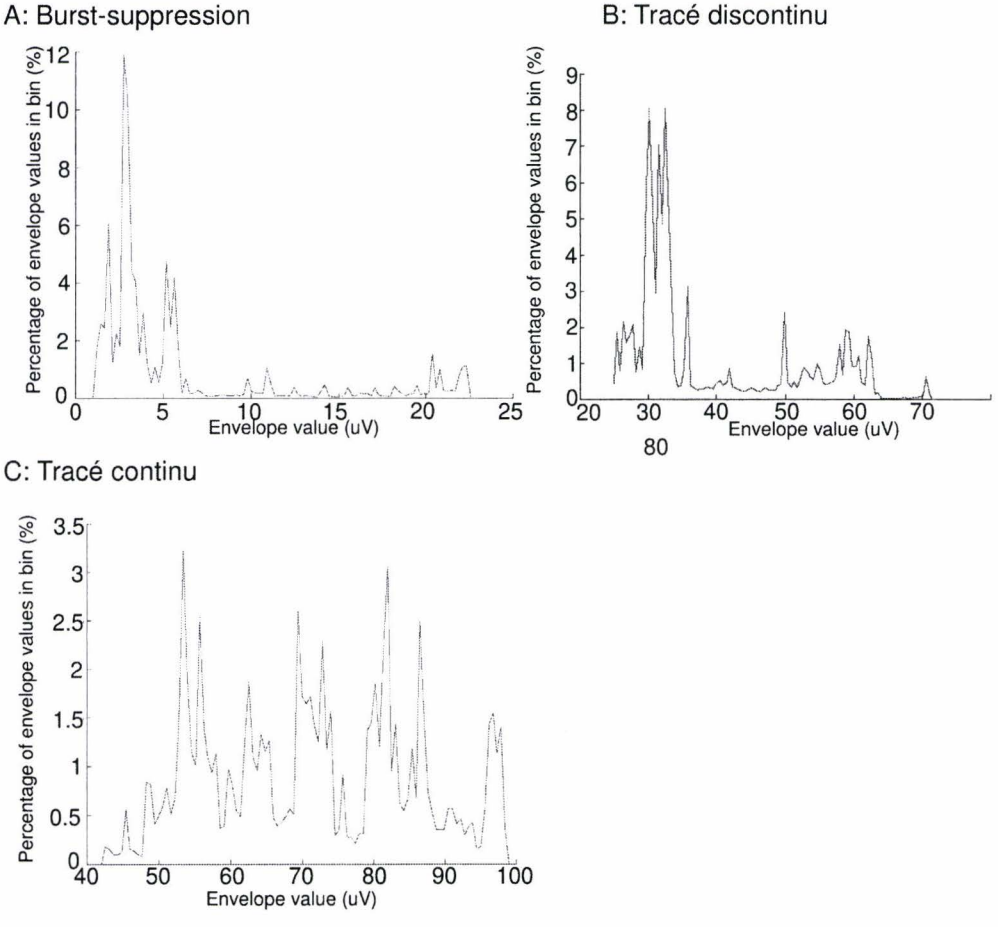

Figure 4.6: *Example of a histogram containing envelope values for a number of background patterns A:burst-suppression B:tracé alternant and C:traé continu*

To differentiate between the other two background types, the envelope value of the bin, that contains most of the envelope values at the left of the histogram is determined. This value will be referred to as the peakvalue. This peakvalue is assumed to represent the mean envelope of the IBIs, which is illustrated in

figure 4.7. Whenever this peakvalue has a value of more than $20\mu V$ the background is marked as tracé alternant. A peakvalue below $20\mu V$ is defined as burst-suppression, according to the definitions given in paragraph 2.3.2.

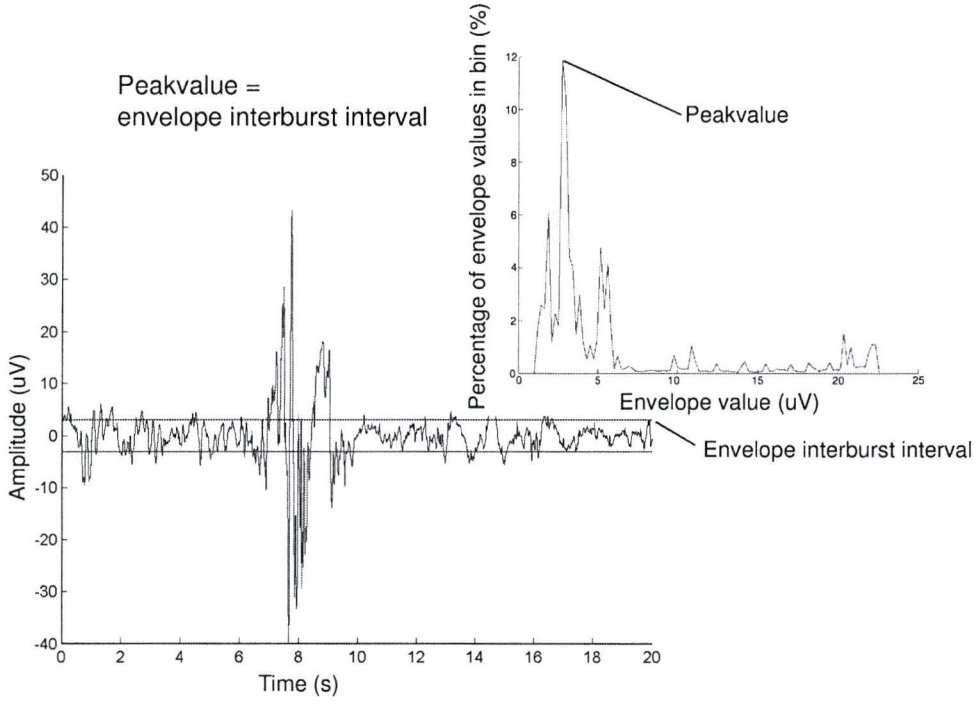

Figure 4.7: *Figure illustrating that the IBI envelope is equal to the peakvalue*

As mentioned, the background classification takes place for all ref-electrode combinations. For each window and reference electrode the number of channels, that are classified as being of a specific background, are saved as a percentage of the total number of combinations, $NrComb$.

4.2.3 Rejection of bad reference electrodes

During this step of the algorithm the background classification percentages per reference electrode are compared to each other. Whenever the percentages of one reference electrode are deviating from the percentages of the other reference electrodes for at least 50% of the windows and with at least a deviation of 50, that reference electrode is rejected. Rejected reference electrodes are not used as reference electrode during the calculation of the burstprobability matrices and are not taken into account when the general background classification is determined.
The procedure to calculate the deviation for a reference electrode will now be explained by means of an example. Consider the matrix shown on the left side of figure 4.8. The matrix is filled with the background classification percentages for three possible reference electrodes at a certain timewindow. First the median values per row are calculated. The median values for the example are shown as the vector in the middle of the illustration. Next, the absolute difference of the percentages in the matrix and the median values are calculated, which results in the matrix shown on the right side of figure 4.8. The deviation per reference

electrode is found by summation of the rows of this difference matrix.

$$\left\| \begin{bmatrix} 50 & 60 & 0 \\ 40 & 40 & 80 \\ 10 & 0 & 20 \\ 0 & 0 & 0 \\ 0 & 0 & 0 \\ 0 & 0 & 0 \end{bmatrix}_{\text{ref1 ref2 ref3}} - \begin{bmatrix} 50 \\ 40 \\ 10 \\ 0 \\ 0 \\ 0 \end{bmatrix}_{\text{median}} \right\| = \begin{bmatrix} 0 & 10 & 50 \\ 0 & 0 & 40 \\ 0 & 10 & 10 \\ 0 & 0 & 0 \\ 0 & 0 & 0 \\ 0 & 0 & 0 \end{bmatrix} + \begin{bmatrix} 0 & 20 & 100 \end{bmatrix} = \text{deviation}$$

Figure 4.8: *An illustrative example of the calculation of the deviation for three reference electrodes*

As can be observed, the deviation for reference electrode three is too high in the example. This reference electrode would therefore be rejected, provided that the deviation remained too high for at least 50% of the windows.
It should be noticed, that this procedure assumes that there is no more than one bad reference electrode, and that the reference electrodes are equally distributed over the left and the right hemisphere.

4.2.4 General background classification

Now that the 'good' reference electrodes have been determined, the separate background classification percentages of these 'good' reference electrodes are combined to a single percentage matrix. This single percentage matrix is calculated by averaging the percentages of the separate percentage matrices. In this way the general background classification is obtained per window of 20 seconds, for instance: low voltage 30% and burst-suppression 70%. This general background classification is illustrated by figure 4.9.

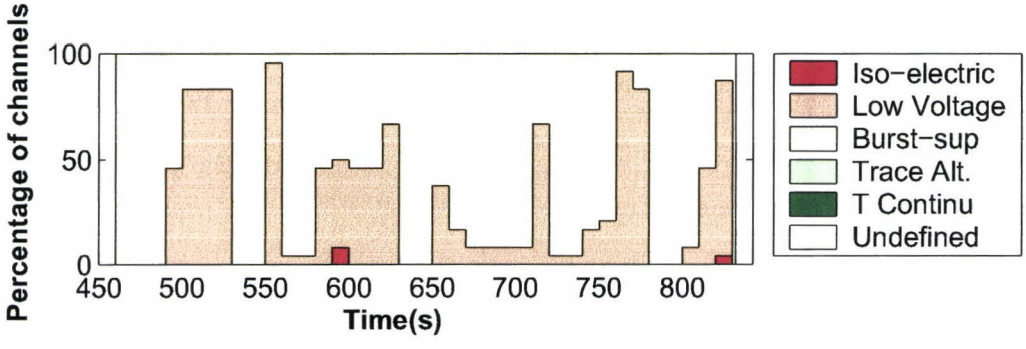

Figure 4.9: *An example of a visual presentation of the general background classification in time as it is generated by the algorithm*

The general background classification is used to determine whether the burst detection algorithm should be carried out for a certain window. If the classification of a burst-suppression background is found for at least two channels, that have been derived from independent electrodes, the burst detection algorithm is carried out for that part of the signal. The criterium of having at least two independent derivations, that are classified as burst-suppression, has been defined to ascertain that a false burst-suppression classification, as a result of a bad electrode, does not cause the burst detection algorithm to be performed.

4.2.5 The burstmatrix and burst detection

Interburst intervals(IBIs) are, according to the definition given in paragraph 2.3.2, periods in which the amplitude does not reach values of $20\mu V$ or more. Consequently a burst period is defined as a period in which the amplitude reaches at least a value of $20\mu V$. The burst detection procedure is based on this definition. A burst is detected whenever the amplitude reaches a value of $20\mu V$ or more. The functioning of this algorithm is illustrated in figure 4.10. The detected bursts are colored blue. The burstlength annotated by the expert is colored red. It should be noticed that, based on this definition, only parts of the annotated bursts are detected, and that bursts are not detected in all channels, that show burst shaped activity. This suggest the setting of some extra criteria for detection.

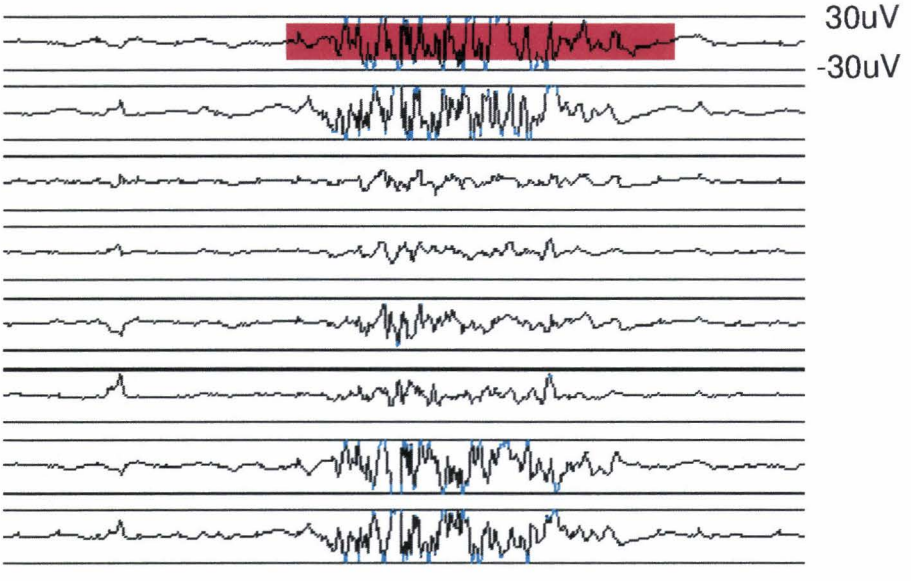

Figure 4.10: *Bursts detected on basis of the definition are shown in blue. The annotated burst is shown in red.*

As can be observed in figure 4.2, the total power increases during bursts. Based on this knowledge a second criterion that enables the detection of bursts in the other channels is laid down. This criterion states that a burst is detected whenever the average total power content exceeds a certain threshold value, $thres$. The average total power content values(APCVs) of the signal are calculated according to the procedure described in paragraph 4.2.2. The threshold value is adaptive, and is defined as:

$$thres = 1/2peakvalue^2 + std(APCVs)/10. \tag{4.4}$$

Here, the peakvalue is equal to the peakvalue as calculated in paragraph 4.2.2. Recall that the peakvalue is assumed to represent the envelope value of the IBIs of the signal. This value is squared and multiplied by $\frac{1}{2}$ to obtain the APCV that represents the IBI. Because there are some small and large scale fluctuations around this APCV, that are not solely caused by burst activity, the second term is added to equation 4.4. This term, the standard deviation of the APCVs divided by 10, is added to distinguish the small, non-burst fluctuations, from larger fluctuations caused by burst activity. The factor 10 is based on practical experience. Threshold values of less than $12.5\mu V^2$ are not allowed. Whenever the calculated threshold value drops below $12.5\mu V^2$ it is automatically readjusted to a value of $12.5\mu V^2$.
After the setting of this additional criterion still only segments of bursts are detected. To be able to detect complete bursts, the segments are enlarged with a procedure similar to the one described for the determination of the precise onsets and endings of movement artifacts. Compared to the procedure for artifacts, onsets and endings have to fulfill a few additional criteria now. These criteria are described in Appendix D.

The bursts detected after the setting of the additional threshold and after the application of the enlargement procedure are shown in figure 4.11.

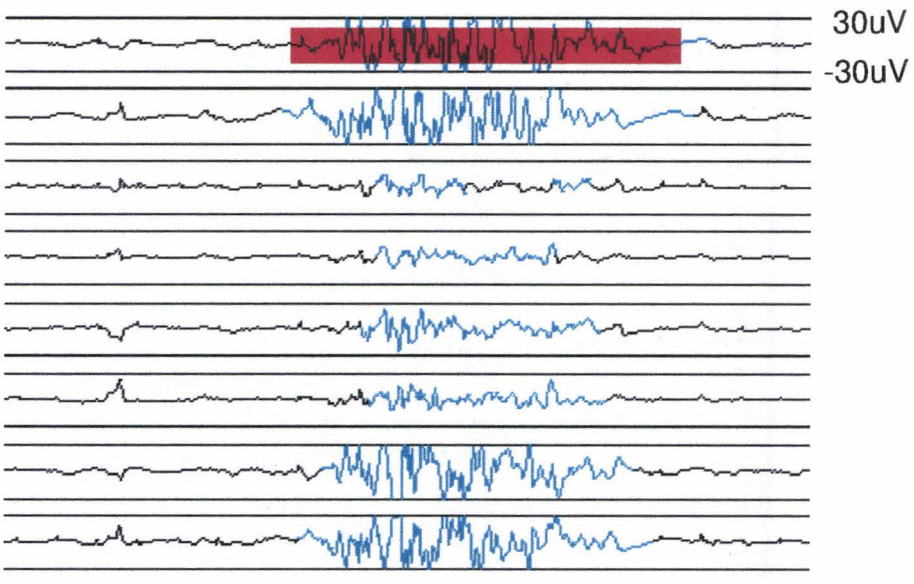

Figure 4.11: *Bursts detected by the algorithm after the setting of of additional criteria are colored blue. The annotated burst is shown in red.*

The bursts and IBIs detected in each channel are saved as a column of a matrix called $BurstMatrix$, which is filled with a 1 for each data point that is identified with burst activity and filled with a 0 for each point corresponding to an IBI:

$$BurstMatrix(i, ch) = 1 \text{ for i corresponding to a burst} \quad (4.5)$$

$$BurstMatrix(i, ch) = 0 \text{ otherwise} \quad (4.6)$$

Whenever burst detection is carried out for a channel whose background pattern is characterized as tracé alternant or tracé continu, the corresponding column is completely filled with ones. Whenever the background of a channel is classified as 'undefined' the row of that channel is completely filled with zeros.
In those cases that the burst detection procedure is not carried out, the matrix $BurstMatrix$ is filled with columns containing solely zeros or ones. Ones in case of a tracé alternant or tracé continu background classification, zeros otherwise.

4.2.6 Burstprobability vectors

Burst activity is generally appearing simultaneously over the entire brain, which is usually not the case for other activity. Therefore the number of channels over which activity is simultaneously detected can be interpreted as a probability that the activity is actually burst activity. These probabilities are calculated for each sample point and saved in the so-called burstprobability vectors. There is one burstprobability vector for each non-rejected reference electrode. To determine the burstprobability at a sample point the number of ref-electrode combinations in which burst activity occurs at that point is divided by the total number of ref-electrode combinations($NrComb$), and multiplied by 100.

4.3 Selecting channels and bursts

The pre-analysis described in the preceding chapter results in the burstprobability vectors, a visual representation of the signal's background pattern and information about whether burst detection should be carried out. The next steps after this pre-analysis are already described in the first paragraph. In short: the channels of interest for further analysis are chosen, the corresponding signals are filtered, and movement artifact detection is performed. Hereafter a burstmatrix is filled according to the procedure described in subparagraph 4.2.5. During the next step it is possible to select only those bursts for analysis, that appear with at least a certain probability for all non-rejected reference electrodes. Consider for instance that only bursts that appear with a minimal probability of 75% are selected for analysis. In that case the probability values saved in the elements of the burstprobability vectors, that correspond to each sample point of the $BurstMatrix$ with a value equal to 1, are regarded. Whenever the probability values of all burstprobability vectors are at least 75% for a specific sample point, that sample point is considered to contain burst activity.
Bursts mostly start with activity in a small area of the brain, that then serves as a trigger for the generation of burst activity in the rest of the brain. The expert from Veldhoven on the terrain of the neonatal EEG claimed that this burst alike trigger should be considered as part of the actual burst. The Neurophysiologist from Nijmegen did however not interpret such triggers as being part of the burst, because of their focal appearance. For this reason an extra option called 'Enable Trigger' is added to the graphical user interface. Whenever this option is enabled, the activity, that is preceding burst activity of a higher probability, is considered to be part of the burst with the high probability.

4.4 Signal analysis

As mentioned the last step of the algorithm involves a thorough analysis of the signal. To this end a number of burst and IBI parameters are calculated.
Some parameters are calculated in the time domain, other parameters are calculated in the frequency domain. For the parameters calculated in the frequency domain first a spectrum of the signal is calculated for each timestep of 0.125 seconds with an STFT procedure. The windowlength is chosen to be 2 seconds, because the lowest frequency component present in the signal after filtering has a frequency of 0.5Hz. The frequency domain parameters calculated are: the average power in the complete EEG frequency range from 0-30Hz, the average power per frequency band, the average relative power of each frequency band compared to the average total power in the EEG frequency range, the average spectral edge, and the average peak frequency. All these parameters are calculated for both bursts and IBIs. The spectral edge is defined as the frequency bin in the spectrum below which 95% of the power in the signal resides. The peak frequency is defined as the frequency corresponding to the frequency bin, that contains the largest part of the signal's power. Each parameter is calculated once per timestep. The final value of each parameter is the average of the values calculated for each timestep. There is one additional parameter calculated from frequency domain information, that requires special attention: the symmetry parameter. This parameter represents the symmetry during burst activity over both hemispheres. It is calculated from the spectra corresponding to a channel of one of the hemispheres and its 'mirrored' channel on the other hemisphere by the contrast function:

$$Sym = \frac{BurstPower_{ch1} - BurstPower_{ch2}}{BurstPower_{ch1} + BurstPower_{ch2}}. \tag{4.7}$$

$BurstPower$ is the summation of the power in the total EEG range during burst activity. An example of a channel on one hemisphere and the corresponding 'mirrored' channel on the other hemisphere is illustrated in figure 4.12.
As mentioned, also a number of parameters are calculated in the time domain. These parameters are: the percentage of burst and IBI is calculated, the shortest burst and IBI, the longest burst and IBI, and the average burst and IBI. Finally, a parameter that expresses the synchronicity in appearance of bursts over both hemispheres is determined. This parameter is calculated by correlation of the BurstMatrix of a channel on one hemisphere with its contra-channel on the other hemisphere. In this way a time shift is determinable, that is presented as the parameter of synchronicity.

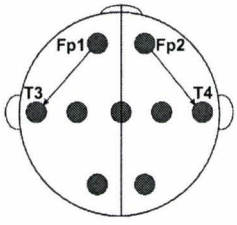

Figure 4.12: *A channel on one hemisphere (Fp2-T4) and its mirrored channel on the other hemisphere (Fp1-T3)*

Chapter 5

Results and discussion

5.1 Background classification

For each segment of 20 seconds of the 10 signals the background pattern with the highest percentage of classification is determined. For instance when the background pattern of a 20 second segment of a signal is classified as a burst-suppression background in 70% of the channels, and as a tracé alternant in the other channels, the background pattern with the highest percentage of classification for that segment is burst-suppression. The number of segments with a certain highest background classification are calculated for each signal and expressed as a percentage of the total number of segments of that signal. These percentages are shown in table 5.1. As mentioned, these general background classifications have been checked by an

Signal	Iso-electric	Low voltage	Burst-sup.	Tracé alternant	Tracé continu
1	90%		10%		
2		80%	20%		
3		25%	75%		
4			100%		
5			90%	5%	5%
6			55%		45%
7			30%		70%
8			25%		75%
9			5%		95%
10				70%	30%

Table 5.1: *Results of the background classification performed by the algorithm*

expert on neonatal EEG recordings from Veldhoven. According to this expert the background pattern was classified correctly in 80 to 85% of the segments. The false classifications are mainly caused by sudden changes in amplitude due to artifacts. Most of the artifacts are caused by medical interventions. An example of a false classification of the background pattern caused by an intervention of the EEG operator is shown in figure 5.1. This background corresponds to signal 1. As can be observed the background pattern has been correctly classified as iso-electric with every now and then short periods of burst-suppression, whenever a peak in amplitude is recorded. These peaks are however not of EEG origin. These peaks correspond to the tapping on the electrodes of the EEG operator. This is performed to confirm that the signal is recorded with a correctly functioning EEG system.
Although it is unlikely that it is possible to develop artifact rejection software for the recognition of such artifacts, there are other artifacts that cause the classification to fail, that could probably be recognized, if the software for artifact rejection would be improved. An example of such an artifact is presented in figure 5.2. This artifact is caused by crying of the newborn and was observed for signal 10. The algorithm falsely interpreted the artifactitious parts of the signal as the periods of large amplitude observed for tracé alternant. As can be observed this artifact manifests itself as high frequent activity. The power of this high frequent activity is however too low to be recognized as movement artifact.

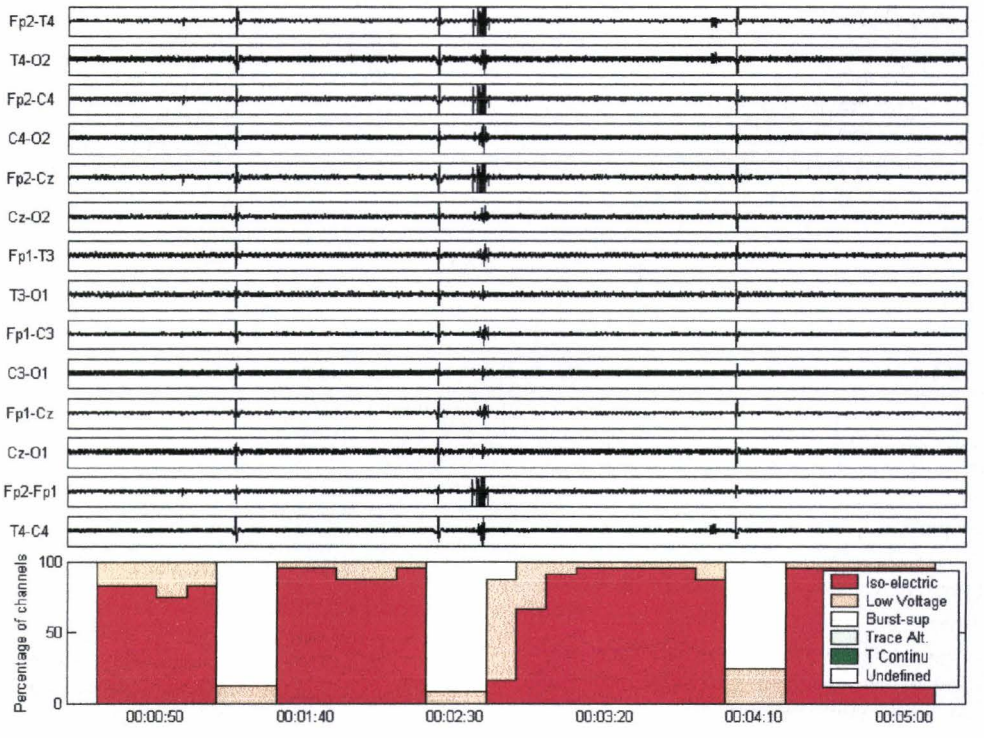

Figure 5.1: *An example of the functioning of the background classification procedure*

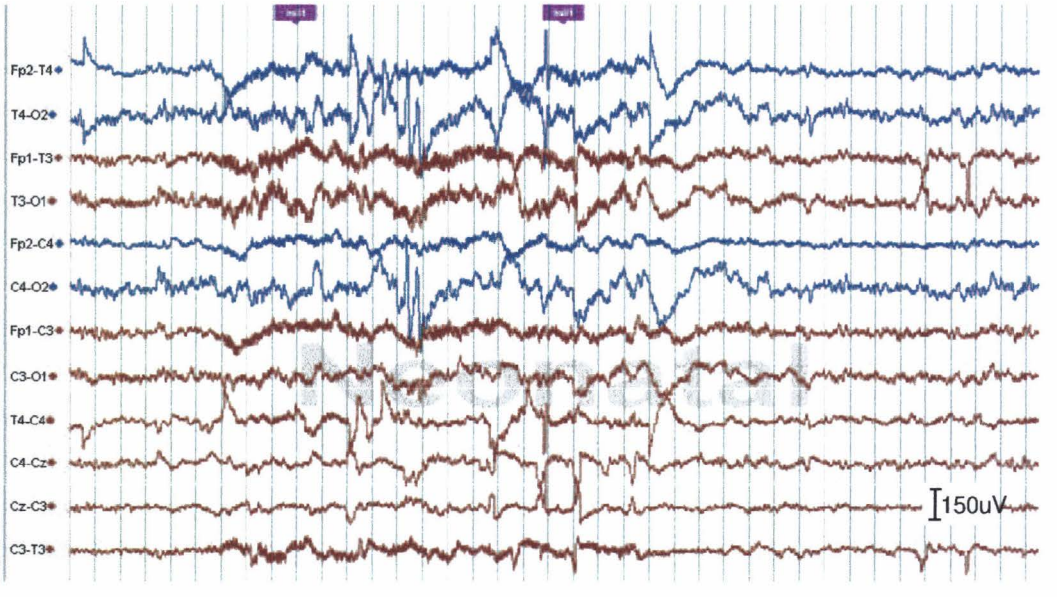

Figure 5.2: *An example of a crying artifact, that is not recognized by the algorithm. This causes the background classification to fail. Each vertical line indicates the start of a new second.*

5.2 Burst detection

For each signal the number of true positives and false positives are calculated. A true positive is noted whenever the algorithm detects burst activity that is at least partially overlapping with one of the bursts annotated by the expert from Nijmegen. A false positive is noted each time the algorithm finds a burst that does not have any overlap with an annotated burst. From the values for the total number of annotated bursts(AB), false positives(FP) and true positives(TP), the sensitivity(S) and positive predictive values(PV) are calculated:

$$S = \frac{TP}{AB} * 100 \tag{5.1}$$

$$PV = \frac{TP}{FP + TP} * 100 \tag{5.2}$$

These parameters are calculated for various settings of the burst detection algorithm. In the first setting only bursts that are simultaneously detected in eight ref-electrode channels are taken into consideration, which corresponds to a burstprobability of 100%. Eight is the maximum number of ref-electrode combinations possible when using the 9-electrode 'baby' configuration. In the second setting also bursts detected in one combination less are taken into account, and so on. The results of the burst detection for the first four settings are presented in table 5.2. The numbers behind TP, FP, S, and PV represent the minimal number of ref-electrode combinations in which a burst should be detected to be taken into consideration.

Signal	Filelength	Nr. of bursts	Nr. of bursts detected															
	(min)	annotated	TP5	FP5	S5	PV5	TP6	FP6	S6	PV6	TP7	FP7	S7	PV7	TP8	FP8	S8	PV8
1	18.75	37	34	4	92	89	33	1	89	97	32	1	86	97	31	0	84	100
2	28.35	53	53	114	100	32	52	86	98	38	49	53	92	48	42	22	79	66
3	30.05	216	215	88	100	71	215	82	100	72	213	58	99	79	204	41	94	83
4	27.97	13	13	13	100	50	12	10	92	55	9	8	69	53	6	2	46	75
5	31.12	153	153	44	100	78	152	28	99	84	150	16	98	90	145	12	95	92
6	20.22	57	57	46	100	55	56	33	98	63	50	22	88	69	38	10	67	79
7	34.33	121	120	46	99	72	120	31	99	79	116	14	96	89	105	7	87	94
8	29.37	26	24	14	92	63	21	10	81	68	18	8	69	69	5	4	19	56
Total	220.15	676	669	369	99	64	661	281	98	70	637	180	94	78	576	98	85	85

Table 5.2: *The number of true positives(TP), false positives(FP), the sensitivity(S), and positive predictive value(PV) found by the algorithm for each recording when taking bursts of different probabilities into account and without setting a criterium for minimal burst length.*

It should be remarked, that the sensitivity of the algorithm is above 80% for all signals when considering bursts that are detected in six ref-electrode combinations or less. In other words bursts detected with a burstprobability of 75% or less. The sensitivity is even above 90% for all signals, except signals 1 and 8. This makes sense because both of these signals show asymmetric burst activity, which causes the recognition of bursts, that do not express themselves in all channels, to be impossible. An example of this asymmetry is shown in figure 5.3. To improve the sensitivity of the algorithm for such asymmetric signals the minimal number of channels, in which burst activity should simultaneously occur to be detected, should be lowered. To make it possible for the algorithm to recognize in which cases asymmetry is present it might be necessary to introduce an initialization period during which the asymmetry parameter described in paragraph 4.4.1 is calculated for a small part of the signal. However, it is expected that this will also increase the false positives found by the algorithm, which means a loss of positive predictive value. To increase the sensitivity with a limited loss of positive predictive value, it might be better to detect a number of large bursts and determine the channels in which they appear with the largest amplitude. Once these channels are determined, the algorithm could separate the periods during which activity is detected simultaneously in this select group of channels from the periods during which activity is detected in other channels. Each period of activity belonging to the first group could than be taken into account as being burst activity.
It should also be noticed that the positive predictive value for signal 2 is low. This is partially caused by false positives that have a duration of less than a second. When setting an additional criterium found in

literature [15], that requires that bursts last for at least a second, the number of false positives decreases, especially for signal 2. The results for the burst detection with this additional criterium are presented in table 5.3.

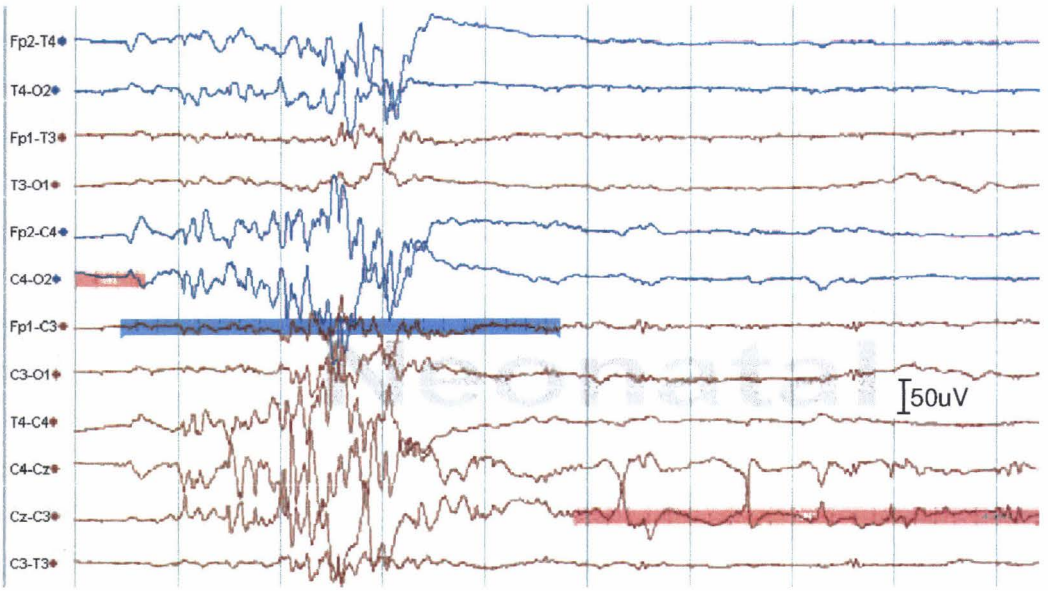

Figure 5.3: *An example of an asymmetric burst. Annotated bursts are colored blue. Annotated other activity is colored red. Each vertical line indicates the start of a new second.*

Signal	Filelength	Nr. of bursts	Nr. of bursts detected															
	(min)	annotated	TP5	FP5	S5	PV5	TP6	FP6	S6	PV6	TP7	FP7	S7	PV7	TP8	FP8	S8	PV8
1	18.75	37	33	1	89	97	32	1	86	97	30	1	81	97	21	0	57	100
2	28.35	53	52	63	98	45	52	41	98	56	42	25	79	63	26	9	49	74
3	30.05	216	212	81	98	72	209	64	97	77	202	33	94	86	170	22	79	89
4	27.97	13	11	7	85	61	8	3	62	73	5	3	38	63	1	2	8	33
5	31.12	153	152	34	99	82	150	21	98	88	144	10	94	94	134	7	88	95
6	20.22	57	51	23	89	69	43	11	75	80	33	2	58	94	13	1	23	93
7	34.33	121	113	11	93	91	103	9	85	92	100	3	83	97	90	1	74	99
8	29.37	26	22	8	85	73	11	6	42	65	7	5	27	58	1	2	4	33
Total	220.15	676	646	228	96	74	608	156	90	80	563	82	83	87	456	44	67	91

Table 5.3: *The number of true positives(TP), false positives(FP), the sensitivity(S), and positive predictive value(PV) found by the algorithm for each signal when taking bursts of different probabilities into account with the additional requirement that bursts last for at least 1 second.*

The overall sensitivity and positive predictive values calculated with and without the 1-second criterium are plotted in figure 5.4. The horizontal axis represents the minimal burstprobability a burst should have to be taken into account.
As can be observed from the preceding tables and figure 5.4 the positive predictive value increased with the setting of the additional criterium. Setting the extra criterium however also has a downside, a relatively large decrease for the sensitivity is observed especially when considering bursts that are detected in 85% or more of the channels. This makes sense because most bursts are only partially detected at this configuration. It is now possible to select one of the sensitivities and its corresponding positive predictive value from the plots of figure 5.4 by setting the criteria for the burst detection. From now on the settings are used, that provide a sensitivity and positive predictive value of 90% and 80% respectively. These values are found in plot B of figure 5.4 when considering bursts that occur in 75% of the ref-electrode combinations. These

settings are chosen for three reasons. First, the one-second criterium seems reasonable, because it is not wished that every short peak in the signal leads to a detection of a burst. Second, the sensitivity and positive predictive value should both be high, which rules out the left and right most points of the plot, leaving the two points in the middle of figure 5.4B to choose from. The preference of the left most point of the two remaining points is based on the philosophy that it is better to detect too many bursts than to miss bursts.

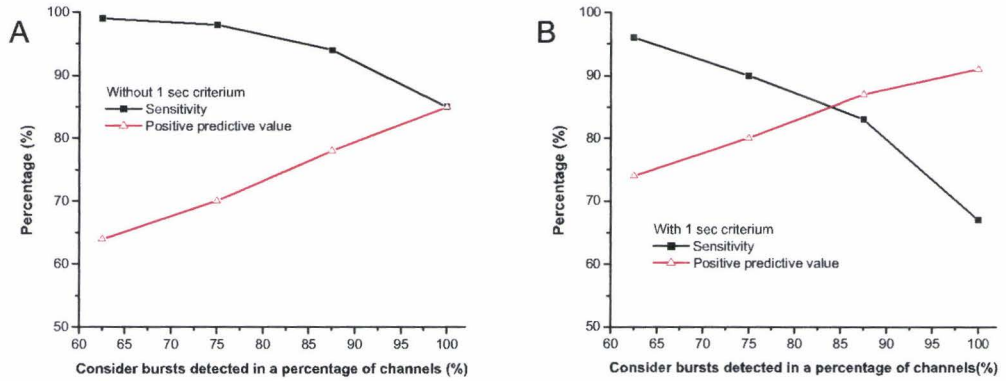

Figure 5.4: *Sensitivity and positive predictive value for the burstdetection algorithm plotted against the probability of the detected bursts. Figure A shows this relation for any detected burst. Figure B shows the relation when only taking bursts of at least 1 second length into account.*

To determine whether the algorithm's sensitivity and positive predictive value are sufficient, it would be best if the inter-observer variability would be known for burst detection. As far as we know there is no literature available in which the annotations of bursts by different observers are compared. To gain some insight in the inter-observer variability in annotating, the expert from Veldhoven has also been asked to annotate signal 1. All of the bursts detected by the expert from Nijmegen have also been annotated by the expert from Veldhoven. However, the expert from Veldhoven annotated 51 bursts more than the expert from Nijmegen. This difference in the number of annotated bursts is mainly caused by a difference in interpretation. The expert from Veldhoven interprets activity appearing in minimal two independent channels as burst activity, whereas the expert from Nijmegen assumes that activity can only be considered as being burst activity, when it appears simultaneously in most of the channels. It is therefore not to be expected that the inter-observer variability is better than the sensitivity and positive predictive value reached by the algorithm. Some of the difficulties encountered when detecting and annotating bursts, are illustrated by figure 5.5. The activity marked with a blue bar is annotated as burst activity by the expert from Nijmegen, the activity colored red is annotated as other activity. As can be observed, the differences in amplitude and frequency are rather small when comparing the burst with the other activity. The algorithm interpreted this other activity as burst activity.

The duration of the detected bursts should be in agreement with the duration of the annotated bursts. This is necessary for a proper determination of parameters like the burstpercentage. To determine whether the duration of the detected bursts is in agreement with the duration of the annotated bursts, first the lengths of the annotated bursts are summed. The resulting burstlength will be referred to as the total burstlength. Next, the duration of the bursts that are correctly detected with the algorithm at a certain probability setting are summed. Because the annotated burst durations are automatically rounded to an integer number of seconds, the burst durations of the algorithm are also rounded to an integer number of seconds for an optimal comparison. The agreement in burst length for different settings of the algorithm is presented in figure 5.6. The vertical axis represents the percentage of the total burstlength that is detected by the algorithm at a specific setting. As can be observed, the best agreement is found when the algorithm takes burstlengths into account that correspond to bursts that occur in at least 62.5% of the channels.

Although the best agreement for the burstlength is found when bursts are considered that appear simultane-

ously in 62.5% of the channels, and the chosen sensitivity and positive predictive value are only achieved when bursts are taken into account that appear simultaneously in 75% of the channels, it is possible to combine the two. To achieve this, the detection of bursts is performed for both the 62.5% and the 75% setting. To reach the desired sensitivity and positive predictive value only the bursts detected at the 75% setting are taken into account. However, because of the underestimation of burstlengths at this setting, the detected bursts are expanded to the length the same bursts have at the detection setting of 62.5%. The burst parameters described in the next paragraph are determined from bursts that have been calculated in this manner.

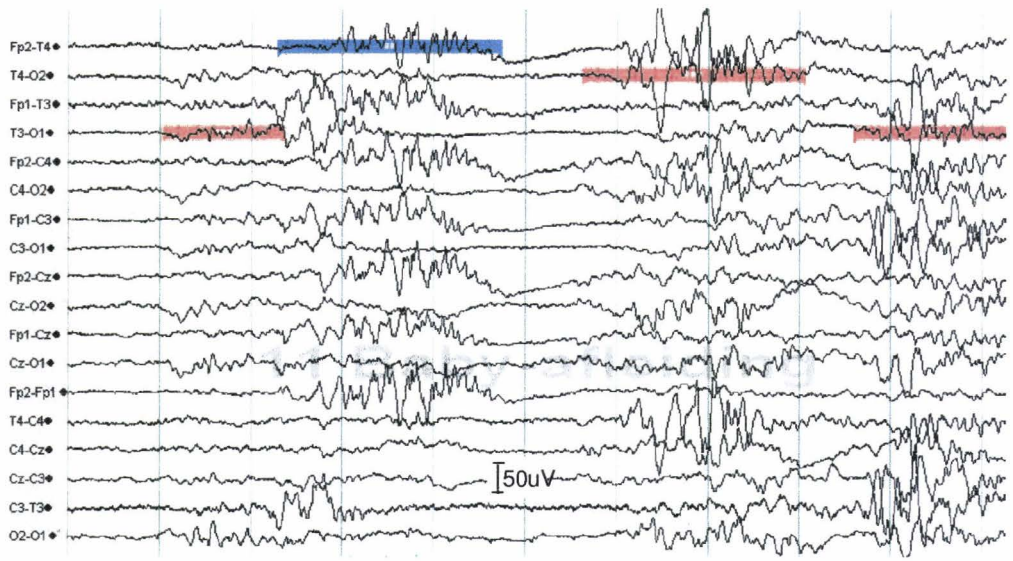

Figure 5.5: *An illustrative example the difficulties encountered when annotating and detecting bursts. Bursts are again annotated with a blue color and other activity is annotated in red*

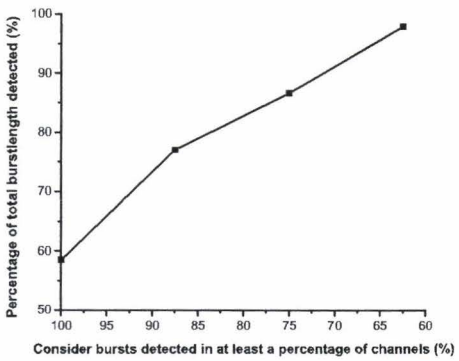

Figure 5.6: *The percentage of total burstlength detected by the algorithm plotted against the burstprobability.*

5.3 Burst parameters

Before calculation of the burst and IBI parameters, the bursts and IBIs are sorted in order of increasing duration. The 5% of bursts and IBIs that are of shortest duration and the 5% of bursts and IBIs that are of longest duration are rejected for the calculation of the parameters. This is carried out to obtain a more representative group of bursts and IBIs. For each parameter, except for the symmetry parameter, the average value and its standard deviation are calculated over three channels per quadrant of the brain. These quadrants and the corresponding three channels are shown in figure 5.7. The averages and standard deviations for each 10 minute segment of the five recordings are shown left in appendices D and E.

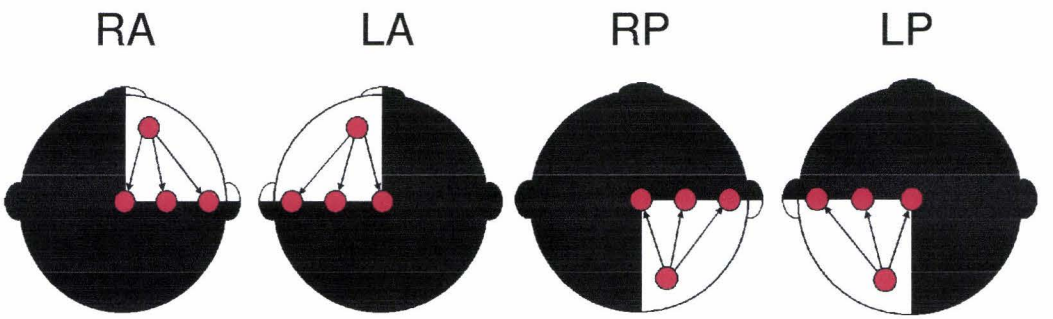

Figure 5.7: *The quadrants and the corresponding channels. RA = Right anterior, LA = Left anterior, RP = Right posterior, LP = Left posterior*

In the figures on the right, the variation of the parameters in time per channel, except for the symmetry parameter, is plotted for each signal. The variation is calculated in percent by dividing the standard deviation of the parameter over the 10 minute segments by the mean value and then multiplying by 100. The variation in time is an indicator of the parameter's suitability for monitoring purposes. A large variation in time means that the parameter calculated over 10 minutes of the signal is not representative for the entire signal and is therefore not expected to be useful as a monitoring parameter, thus a low variation in time is wanted. It should however be remarked, that the timescale over which the parameter is calculated, is of importance. A parameter is likely to show less variation when calculated over a larger part of the signal and therefore it might be that a parameter calculated per 10 minutes of a signal shows a lot variation, whereas the same parameter calculated over 20 minutes of the signal shows little variation in time and is representative for the entire signal.
The variation in time and place for each category of parameters is discussed next.

Parameters related to a specific frequency

As can be observed on the left in figure D1, the spectral edge parameter has values of about 10Hz for burst periods, except for recording 3, that has a spectral edge value of about 4Hz. Remarkable is that recording 3 belongs to the only patient of the group that passed away shortly after birth. The low value could however also be an effect of medication. This patient received fenobarbital, midazolam, and morfine. The time variation of the average spectral edge parameter for bursts is generally less than 20%, which corresponds to a change of 2Hz at the frequency of 10Hz. In spite of this variation in time, the low value of recording 3 is still distinguishable and therefore this parameter is expected to be suitable for monitoring.
The average peak frequency values for bursts do not vary much in time and place, in general variations of less than 20% are observed. This parameter is therefore considered usable for monitoring. The peak frequency values calculated are in the range of 0.7 to 3.3Hz.
The average spectral edge values found for the IBIs are in the range of 10Hz to 25Hz. The variation in time is about 20%, which is rather small. This means that the parameter calculated over 10 minutes of the signal in a single channel is representative for the entire signal in that channel. The large variations observed in place imply that the parameter is only representative for one channel. Perhaps this parameter provides local information about the development of the child. A remark should however be made about all the frequency

related parameters of the interburst intervals. The prognostic value of these parameters is to be doubted because of the much lower signal to noise ratio for these periods.
The time variation of the average peak frequency values for interburst intervals is more than 20% in the anterior areas and less than 20% in the posterior areas. At best this parameter would be useful in providing information about the posterior areas however because of the remark about the low signal to noise ratio this parameter is not rejected as a valuable monitoring parameter.

Time domain parameters

The burstpercentage parameter shows very little variation over the various areas of the head, which is as expected because only bursts appearing in at least 75% of the channels are taken into account. The variation in time of about 40% and 30% for channels one and three seems rather high, however because the absolute values for the burst percentages are also low, about 1.2% and 9%, the absolute variation in time is still small, about 0.5% and 3%. Therefore this parameter might be useful as a monitoring parameter.
The shortest burst parameter is not expected to be a parameter useful for monitoring, both variations in time and place are large.
The longest burst parameter seems to be a more suitable parameter for monitoring, place variation is small for all recordings, except for recording four. Time variation is also small for recordings 2,3 and 5. The detection of enormous burst lengths of 25 seconds for recording 4 is probably caused by the presence of short IBIs of about a second. The algorithm is not capable of separating different bursts and instead one large burst is detected. An example of two separate bursts 'glued' together from recording 4 is shown in figure 5.8. This probably also causes the enormous variation in time of the parameter for that signal. The large variation in time of recording 1, which is also observed for the average and shortest burst parameter, is probably caused by the fact that the number of bursts available within the ten minutes for the determination of the parameter is too little.

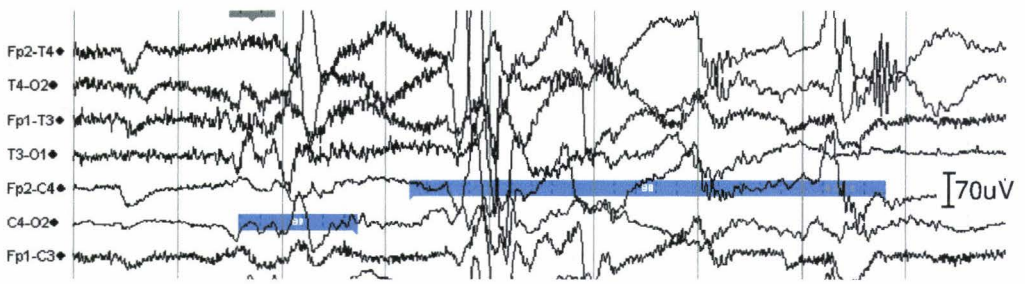

Figure 5.8: *Two bursts that are detected as being a single burst by the algorithm due to the short IBI in between*

The average burstlength parameter is probably the best of the three burstlength parameters plotted. It has both a low variation in time and in place. However, the average burst duration is also influenced by the 'gluing' problem. To obtain information about burst durations, which is least dependent of 'glued' bursts, it might be better to use a parameter, that is defined as the burstlength most often encountered in a signal. This parameter could be calculated from a histogram of burstlengths.
The two most suitable time domain parameters of the interburst intervals are the IBIpercentage and the average IBI length, because of their low variation in time. However, because the IBIpercentage is one minus the burstpercentage, one of these parameters is redundant. The average IBI length parameter has the lowest variation in time of the three IBI length parameters and is therefore most suitable for monitoring. However, also for interburst intervals a parameter, that is defined as the interburst interval length most often encountered in a signal, might quantify the interburst interval's length better.
A recommendation in order to improve the determination of the burst and IBI length parameters is to calculate the parameters on basis of a predefined number of bursts or IBIs and not on basis of a time segment of the recording. In this way the parameters for recordings with a small number of bursts or IBIs

per unit of time, like recordings 1 and 3, can be compared more fairly to the parameters calculated for a signal with many bursts or IBIs per unit of time, like recordings 2,4 and 5.

Relative power parameters

In general, the variation in space of the relative power parameters for bursts is showing less variation in the anterior areas than in the posterior areas. The variation in time of the relative δ-power parameter is lowest, it is below 10% for all recordings, except for recording 1. A low rate of variation in time for the relative δ-power was also described in literature [16]. The variation in time for recording 1 might become less, when more bursts are taken into account. It should be recalled that the burstpercentage for this signal was about 1%, whereas it was at least 10% for the other signals. For a fair comparison of power related parameters over the five recordings it would had been fairer if they were calculated over an equal length of bursts. As can be observed, the power of the spectrum of a newborn is mainly distributed over the δ and θ bands. This is also found in literature [16]. The relative power parameter best suitable for monitoring is the δ band for both bursts and interburst intervals, because of its low variation in time.

Absolute power parameters

The absolute power parameters for both bursts and IBIs vary too much in time and space to be used for monitoring purposes. It should be noticed, that the powers detected in the anterior part of the brain, during bursts, are much higher than in the posterior part for all patients, except for recording 3. The contrary was found in literature [13]. For recording 3 most power is found in the left posterior part of the brain, which is in agreement with a statement in the EEG report of the recording, that the bursts seemed to be of higher amplitude on the left side of the brain.

Symmetry

The symmetry parameter has been calculated for the eight channels on the right hemisphere with respect to the corresponding eight channels on the left hemisphere. It has not only been determined per time segment of 10 minutes of the five recordings, but in addition it has also been calculated for 10 minutes of two recordings, that had been reported as being asymmetric. The first has an asymmetry towards the right hemisphere and the second has an asymmetry towards the left hemisphere. The results are plotted in figure 5.9.

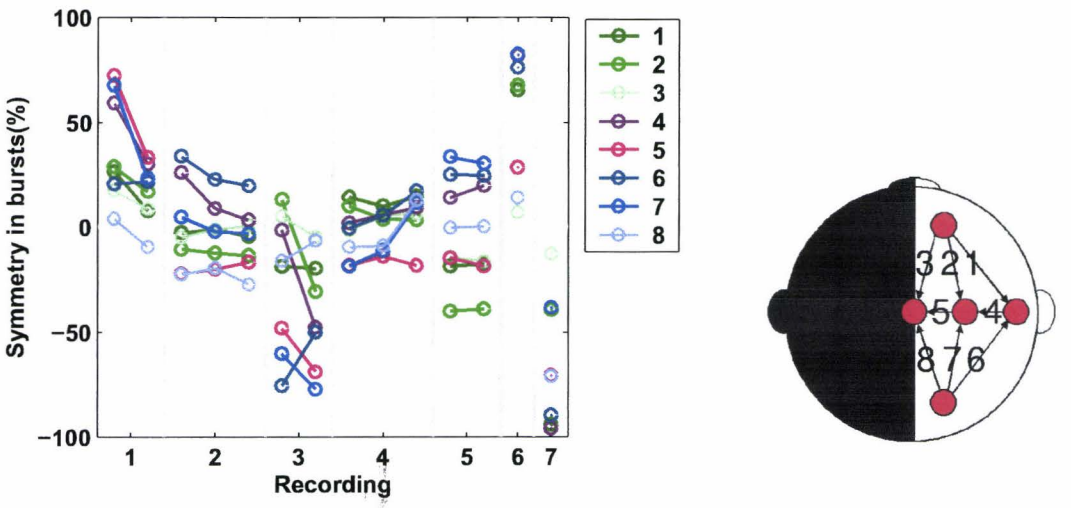

Figure 5.9: *The symmetry parameter for the five recordings plus a recording with asymmetry towards the right and the left hemisphere respectively.*

The results for the channels in the anterior part of the right hemisphere are colored green and the channels in the posterior part of the right hemisphere are colored blue. The darker the color, the further the channel is located from the sagittal midline.
As can be observed, the symmetry parameter reflects the asymmetry clearly for the additional recordings. Also for recording 3 the slight asymmetry towards the left in the posterior areas is reflected by the parameter. It should be noticed that the asymmetry expresses itself best in the channels that are further away of the sagittal midline. This makes sense, because these channels are separated by a longer distance from their opposites on the left hemisphere. The further the distance between channels, the less the signal of the first channel is influenced by the signal of the other channel. It is therefore best if the asymmetry is determined from channel combinations like Fp2-T4(1) and Fp1-T3, and O2-T4(6) and O1-T3. In literature a parameter of symmetry is often defined for one channel only, which is expected to reflect asymmetry over the entire brain. However, as can be observed for recording 3, it is not necessary that asymmetry expresses itself both in anterior areas and in posterior areas. Therefore a separate symmetry parameter for the posterior part and the anterior part of the brain is recommended.

Summary and general discussion

The parameters that are considered to be most useful for monitoring purposes are in the time domain: the percentage of bursts, and the average length of IBIs and bursts. In the frequency domain the parameters most suitable for monitoring are: the average spectral edge, the average peak frequency, and the average relative amount of delta power in the burstperiods of a signal. Segmentation of the signal in segments of a certain length is however probably not the best way to calculate a parameter, except for the burstpercentage parameter. For a fair comparison of parameter values it would be better to calculate the frequency parameters from the same amount of burst time and to determine the burst and IBI length parameter from an equal amount of bursts and IBIs for each signal.
If the number of electrodes needed for the quantification of the newborn EEG could be reduced to five electrodes, the discomfort for the newborn would be lowered. Furthermore it would be less time consuming for the EEG operator to attach the electrodes. As can be observed in the figures on the left of appendices E and F, the variation of the 'suitable' parameters in place over each quadrant is in general less than 20% of the parameter's value. For the determination of parameters like the percentage of time occupied by burst activity, the number of electrodes could possibly be reduced to five, one in each quadrant and the Cz electrode. However, for monitoring the pair of symmetry parameters already six electrodes are needed, Fp1, Fp2, T3, T4, O2 and O1. If these symmetry parameters where to be measured simultaneously with the burst percentage parameter already seven electrodes would be needed. A reduction from nine electrodes to seven might therefore be an option. To claim that seven electrodes provide all the information needed, additional research is needed. Finally, it should be remarked that the rejection of the electrodes C4 and C3 would imply a reduction in the number of possible reference electrode combinations. This might cause a decrease in functionality of the algorithm.

Chapter 6

Conclusions and recommendations

It is possible to automatically classify the background signal of an EEG registration of a full-term newborn by mathematically defined parameters per 20 second signal. A proper validation procedure should be performed before clinical application. For a proper validation, two experts in interpreting EEG signals of newborns should be asked to determine the background signal of EEG channels for segments of 20 seconds for a large number of EEG recordings. Afterwards the classifications given by the experts should be compared to each other and to the algorithm. The sensitivity and specificity of the algorithm should be comparable to, or better than the correlation between the two experts.
The background classification can be improved through further development of the automatic artifact rejection software. To gain more insight in the characteristics of artifacts, which allows the development of the software for the automatic rejection of artifacts, annotating by the EEG operator and the nursing staff during medical interventions is necessary.
For monitoring purposes a translation of the presentation of the background pattern classification in the time domain to a presentation in space by use of a brainmap would also be useful. It would create the opportunity to compare the background patterns to MRI images.
It is concluded that it is also possible to automatically separate burst and suppression periods of a burst-suppression pattern with a sensitivity of 90% and a positive predictive value of 80% compared to the annotations of an expert by use of the developed algorithm. To determine whether the sensitivity and positive predictive value are sufficient for clinical usage, the annotation of bursts should be performed by a second expert. The correlation between the algorithm and each of the observers should be similar to, or better than the correlation between the two observers.
The percentage of time occupied by bursts, the average duration of bursts and interburst intervals, the relative amount of power in the delta band, the symmetry of the posterior areas, the symmetry of the anterior areas, and the average spectral edge and average peak frequency during bursts calculated over 10 minute segments are considered to be the most suitable parameters for monitoring applications.
The exact prognostic significance of these parameters has to be proven in future clinical studies. A project focussing on the differences in the values of the described burst and IBI parameters for groups of full-term newborns with varying pathologies, or a project focussing on the change of the burst and IBI parameters during the maturation of the brain is advised.
If possible it would also be valuable to investigate the effect of medication and the dose of medication on the EEG signal of the newborn.

Appendix A

The normal EEG

A.1 Background patterns

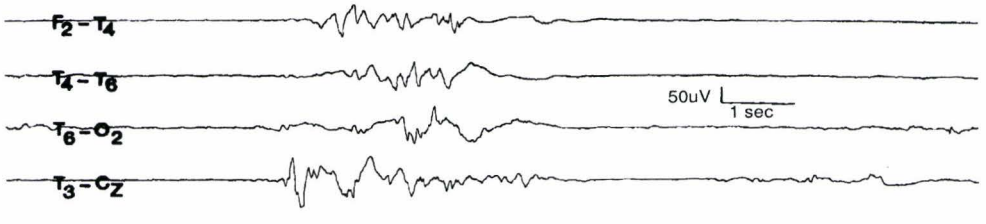

Figure A.1: *Tracé discontinu [6]*

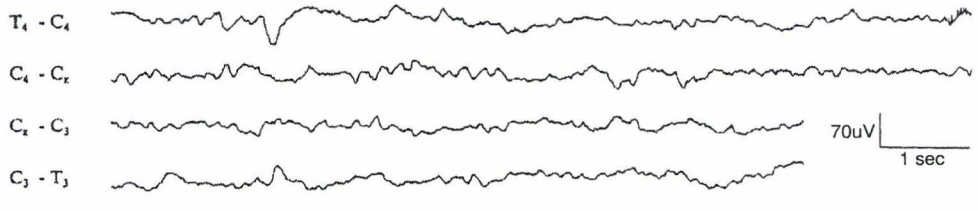

Figure A.2: *Tracé continu [6]*

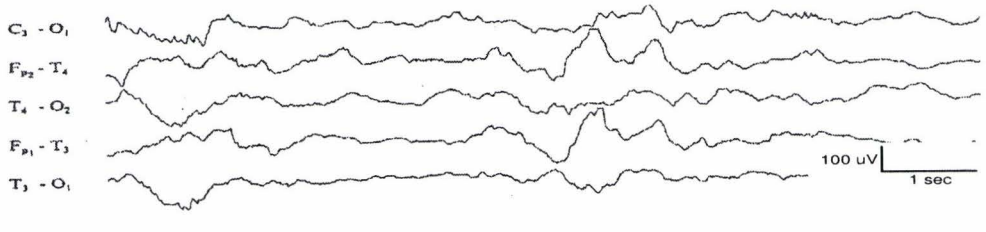

Figure A.3: *Tracé alternant [6]*

A.2 Age related patterns

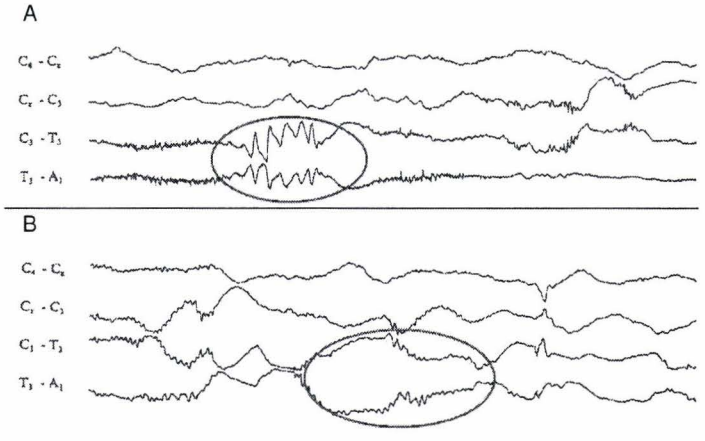

Figure A.4: *A:an example of a temporal sawtooth, B:an example of a delta brush*

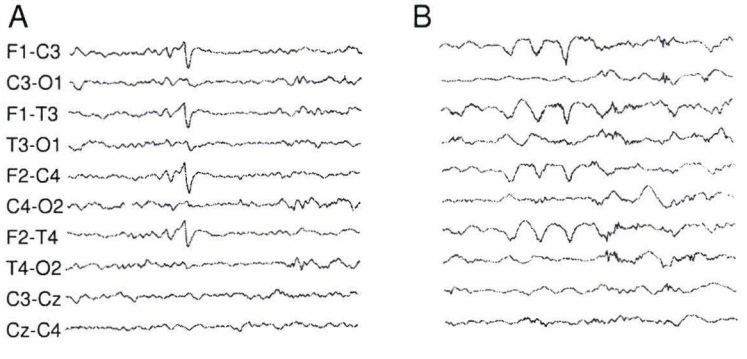

Figure A.5: *A:an example of encoches frontales, B:an example of anterior slow dysrhythmia [17]*

Appendix B

The abnormal full-term EEG

B.1 Abnormal background patterns

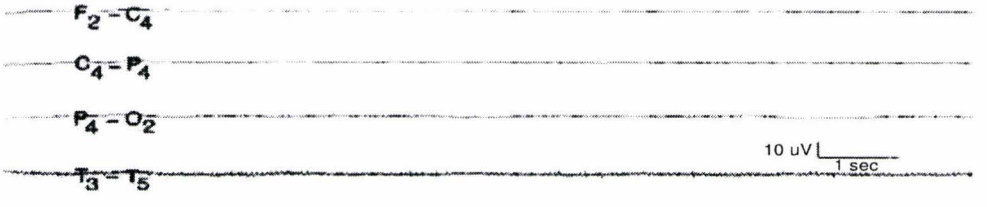

Figure B.1: *Iso-electric background pattern [6]*

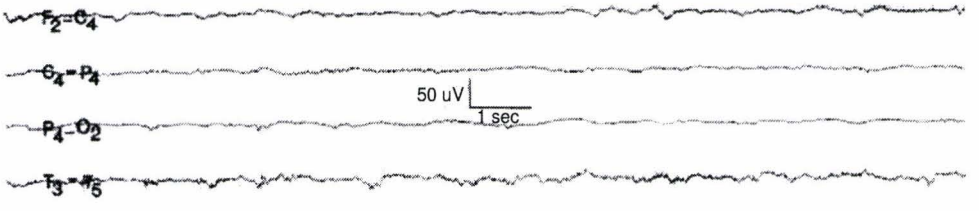

Figure B.2: *Low voltage background pattern [6]*

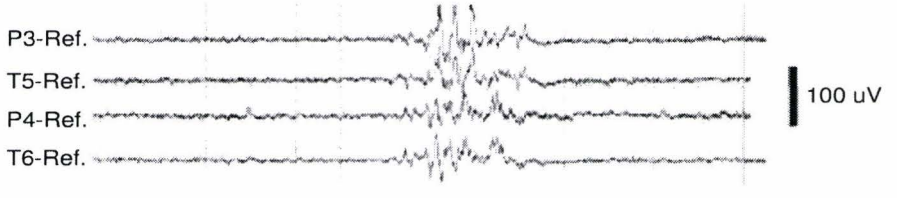

Figure B.3: *Burst-suppression background pattern [13]*

B.2 Abnormal patterns

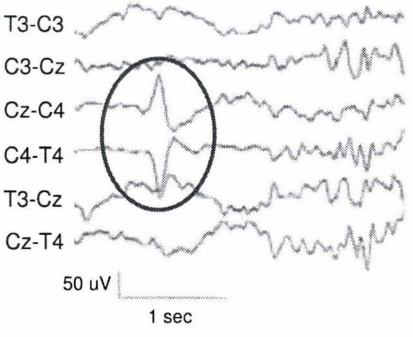

Figure B.4: *An example of a positive rolandic sharp wave [5]*

Appendix C

EDF/EDF+ file format

Header record 256 bytes			
Bytes	**Description**	**Data type**	**Comments**
0-7	Version of data format	ASCII	0
8-87	Patient identification	ASCII	Separated by spaces: PIN, sex(M/F) birthdate(dd-MM-yyyy), patients name[1]
88-167	Recording identification	ASCII	Separated by spaces: 'Startdate', startdate (dd-mm-yyyy), investigation code, operator code, equipment code
168-175	Start date recording	ASCII	dd.mm.yy (clipping date: 1985)
176-183	Start time recording	ASCII	hh.mm.ss
184-191	Number of bytes in header record	ASCII	
192-235	Reserved	ASCII	Must start with 'EDF+C' if recording is uninterrupted and 'EDF+D' if recording is interrupted
236-243	Number of data blocks	ASCII	
244-251	Duration of a data block[s]	ASCII	A data block should not contain more than 61440 bytes
252-255	Number of signals(ns)	ASCII	
Signal header record ns·256 bytes			
Bytes	**Description**	**Data type**	**Comments**
0-(ns·16-1)	ns·label	ASCII	e.g. EEG O1-O2
ns·16-(ns·96-1)	ns·transducer type	ASCII	e.g. AgAgCl electrode
ns·96-(ns·104-1)	ns·physical dimension	ASCII	e.g. uV
ns·104-(ns·112-1)	ns·physical minimum	ASCII	e.g. -500
ns·112-(ns·120-1)	ns·physical maximum	ASCII	e.g. 500
ns·120-(ns·128-1)	ns·digital minimum	ASCII	e.g. -2048
ns·128-(ns·136-1)	ns·digital maximum	ASCII	e.g. 2048
ns·136-(ns·216-1)	ns·prefiltering	ASCII	e.g. HP:0.1Hz LP:75Hz
ns·216-(ns·224-1)	ns·nr of samples per block	ASCII	
ns·224-(ns·256-1)	ns·reserved		

Table C.1: Edf header format. [1]*Any space inside the content of these subfields must be replaced by a different character, f.i. an underscore. Subfields whose contents are unknown, not applicable or must be made anonymous are replaced by a single character 'X'*

The file format supports interruption of data by means of the 'EDF annotations' signal. This is a signal stored in the data record that has the label 'EDF annotations' with annotations as time-stamped annotations

Data record			
Bytes	**Description**	**Data type**	**Comments**
nr of samples[1]·2	First signal in data record	16 bits integer	
nr of samples[2]·2	Second signal in data record	16 bits integer	
...			
...			
nr of samples[ns]·2	Last signal in data record	16 bits integer	

Table C.2: Edf data record format

lists (TALs). Each TAL starts with a time-stamp that specifies the time (in seconds) that the onset of the annotated event follows or precedes the start time of the file and the duration of the annotated event (also in seconds). Onset and duration are coded using US-ASCII characters with byte values 43, 45, 46, 48-57 ('+', '-', '.' and '0'-'9'). Onset must start with a '+' or '-' character, and both onset and duration can contain a '.' to specify fractions of a second. Duration is preceded by byte value '21' and followed by byte value '20'. Duration can be skipped, in which case its preceding '21' must also be skipped. After the time stamp, a list of annotations all sharing the same onset and duration may follow (in US-ASCII character bytes). Each annotation is followed by byte value '20' and the last '20' of a TAL is followed by byte value '0'. In each data record, the first TAL must start at the first byte of the 'EDF Annotations signal'. Subsequent TALs in the same data record must follow immediately after the trailing of the preceding TAL. A TAL, including its trailing, may not overflow into another data record. Each event is annotated only once, even if its duration makes it extend into the time period of other data records. Unused bytes of the 'EDF annotations' signal in the remainder of the data record are filled with byte value '0'. For EDF compatibility, the fields 'digital minimum' and 'digital maximum' must be filled with -32768 and 32767, respectively. The 'physical maximum' and 'physical minimum' fields must contain values that differ from each other. The other fields of the 'EDF annotations' signal are filled with spaces.

Appendix D

Criteria for burst enlargement

The minima in total power that indicate onset and ending of a burst have to correspond to an APCV, that is at least $12.5\mu V^2$ and maximal equal to $maximum$, provided that $maximum$ has a value larger than $12.5\mu V^2$. The variable $maximum$ is defined as:

$$maximum = 1/2peakvalue^2 + 1/50 * std(APCVs), \tag{D.1}$$

The reason for setting this extra criterion is to make sure that not every minimum is regarded as a possible onset and ending of the burst, which would lead to a detection of only a small part of each burst. The $maximum$ makes sure that the average power content in the signal first has to be decreased to a respectable small value. The demand that $maximum$ is at least equal to $12.5\mu V^2$ assures that the $maximum$ value does not drop too low, which might cause the algorithm to overestimate the duration of burst periods. Finally, the burst onset has to be corrected for the hysteresis shift caused by the windowing. In this case the shift that needs to be corrected for measures 1 second. As a consequence of the usage of 1-second-windows it is therefore only possible to separately detect bursts that have been separated by an IBI of at least 1 second time length.

Appendix E

Burst related parameters

On the left side plots are shown, that describe the variation of a burst related parameter over various regions of the head. On the right side the variation in time of each parameter per EEG channel is shown. Next to this also the average of these variations over all channels is plotted in black with its standard deviation. Each triangular shaped point correspond to a different specific channel. The colors of the triangular points correspond to a specific channel. The color corresponding to each channel is illustrated by the figure at the end of this Appendix. Similar pairs of plots for parameters related to the interburst intervals(IBIs) are shown in the next appendix.

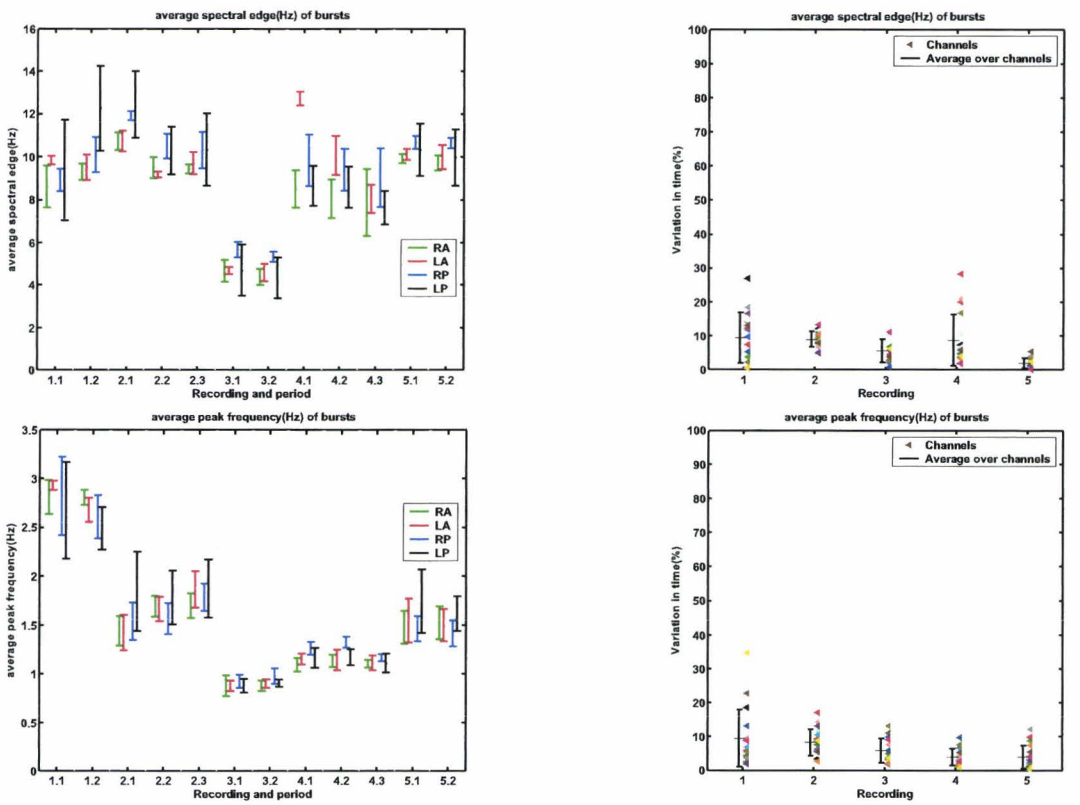

Figure E.1: *Parameters related to a specific frequency*

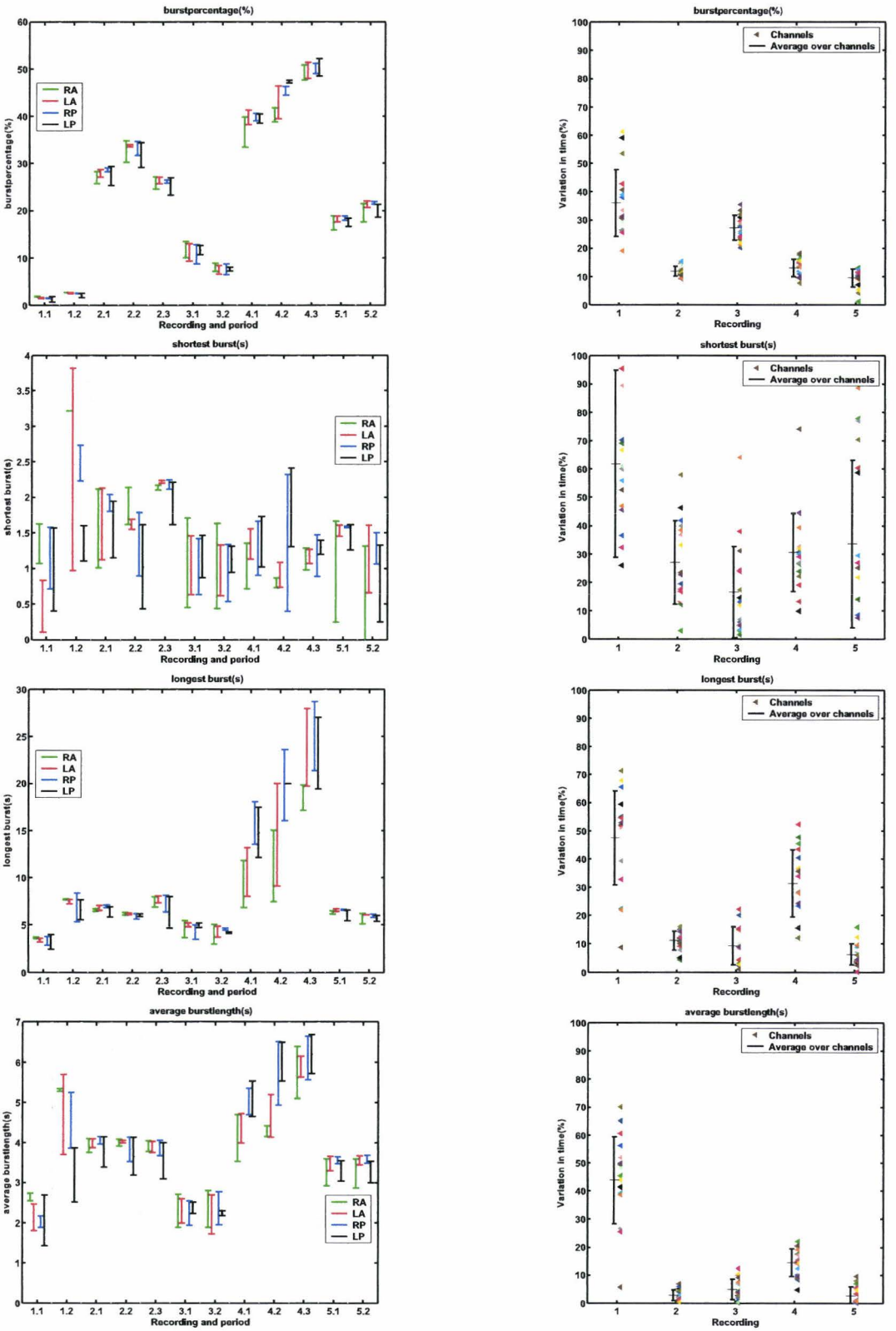

Figure E.2: *Time domain parameters*

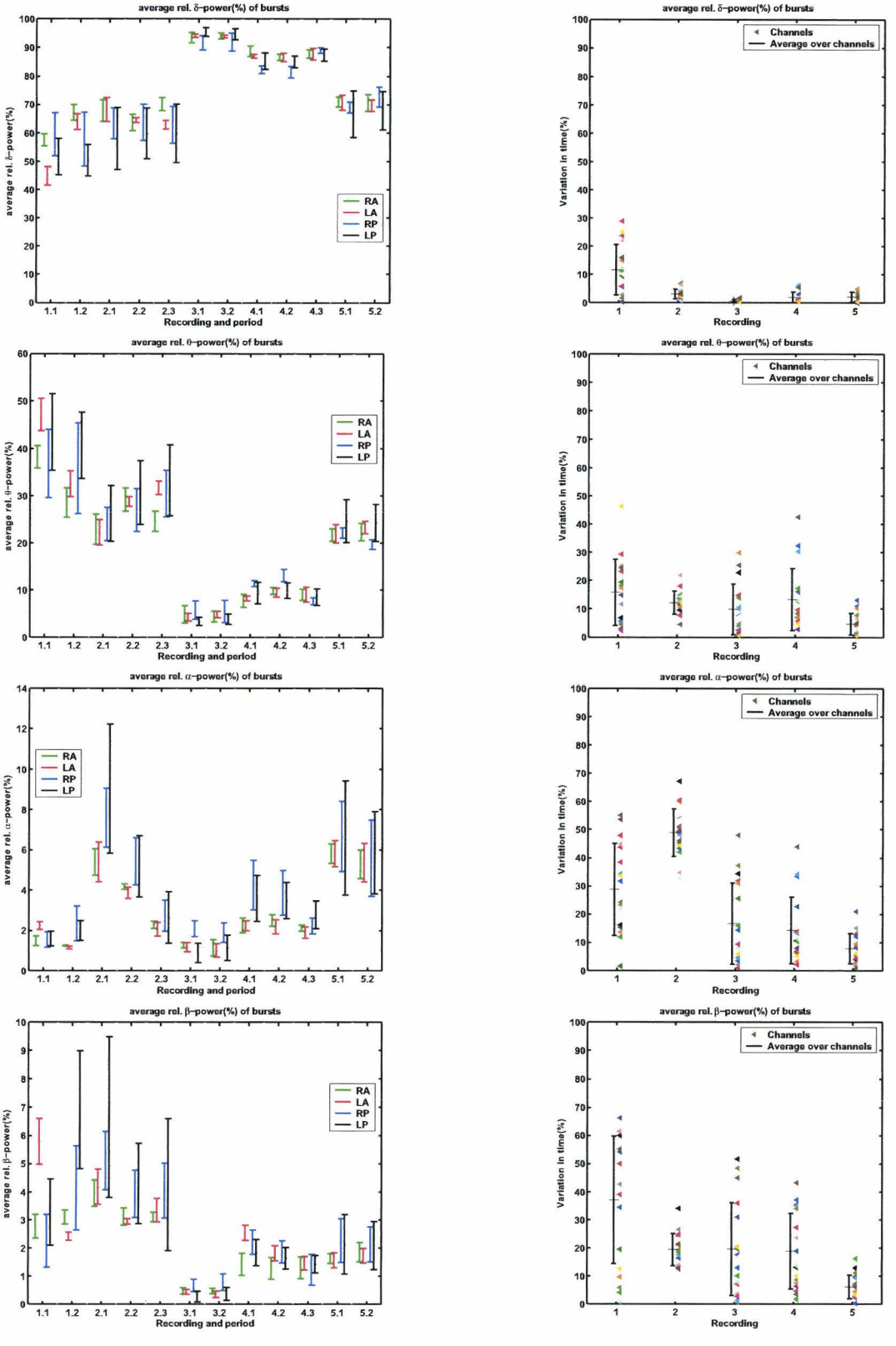

Figure E.3: *Relative power parameters*

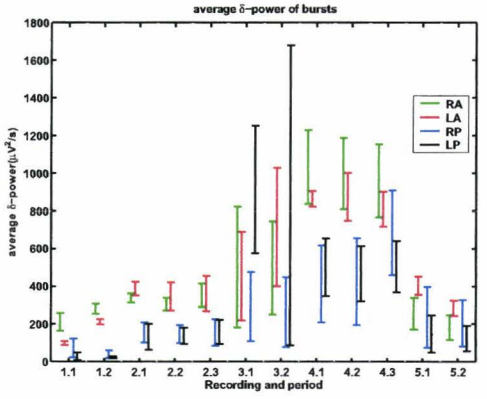
average δ-power of bursts
average δ-power(μV²/s)
RA
LA
RP
LP
1.1 1.2 2.1 2.2 2.3 3.1 3.2 4.1 4.2 4.3 5.1 5.2
Recording and period

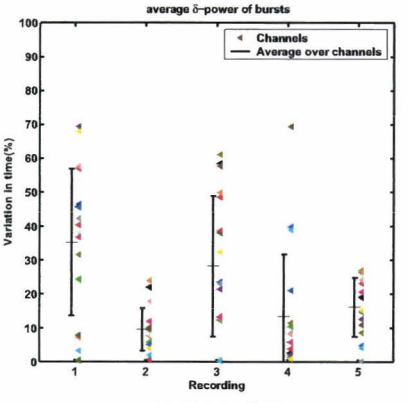
average δ-power of bursts
Channels
Average over channels
Variation in time(%)
1 2 3 4 5
Recording

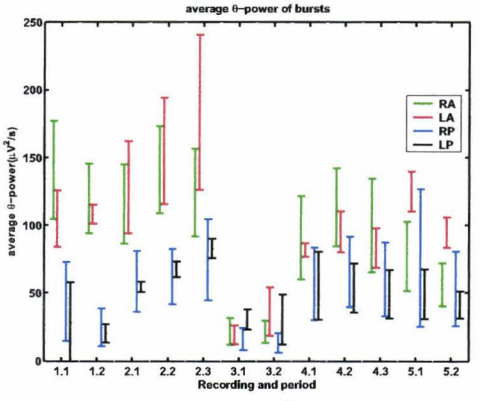
average θ-power of bursts
average θ-power(μV²/s)
RA
LA
RP
LP
1.1 1.2 2.1 2.2 2.3 3.1 3.2 4.1 4.2 4.3 5.1 5.2
Recording and period

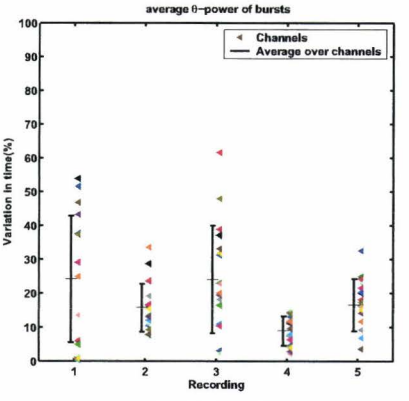
average θ-power of bursts
Channels
Average over channels
Variation in time(%)
1 2 3 4 5
Recording

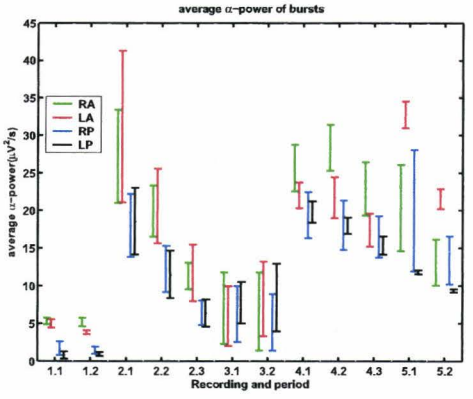
average α-power of bursts
average α-power(μV²/s)
RA
LA
RP
LP
1.1 1.2 2.1 2.2 2.3 3.1 3.2 4.1 4.2 4.3 5.1 5.2
Recording and period

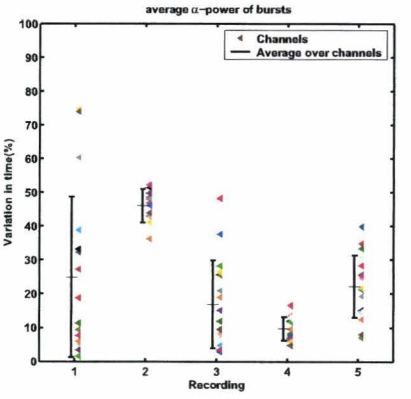
average α-power of bursts
Channels
Average over channels
Variation in time(%)
1 2 3 4 5
Recording

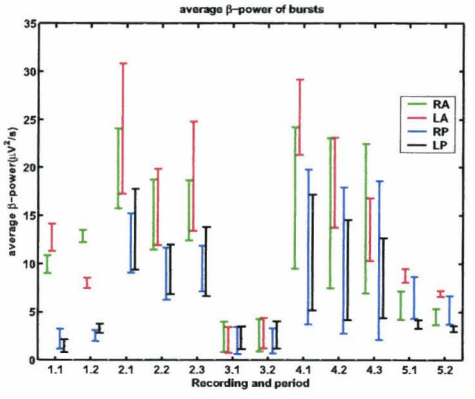
average β-power of bursts
average β-power(μV²/s)
RA
LA
RP
LP
1.1 1.2 2.1 2.2 2.3 3.1 3.2 4.1 4.2 4.3 5.1 5.2
Recording and period

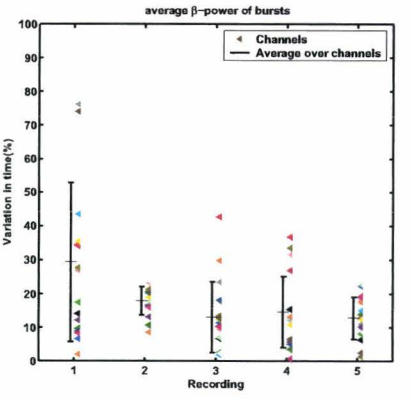
average β-power of bursts
Channels
Average over channels
Variation in time(%)
1 2 3 4 5
Recording

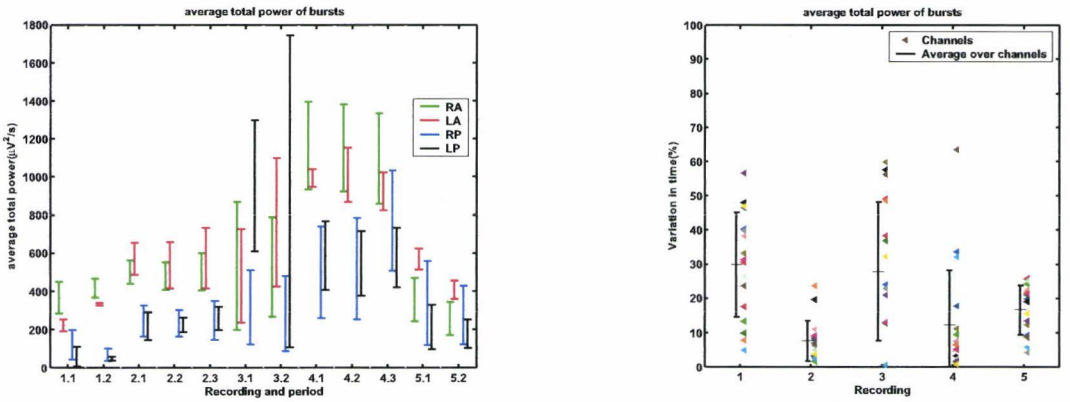

Figure E.4: *Absolute power parameters*

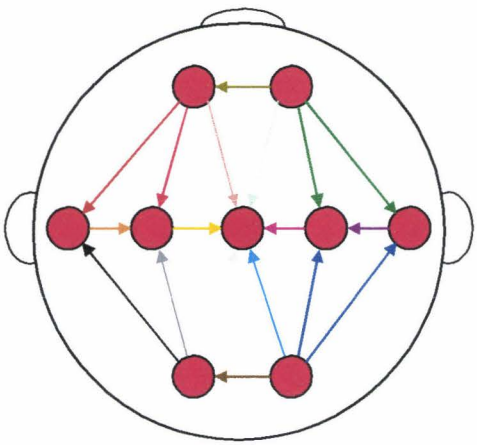

Figure E.5: *A schematic overview of the colors used for the data points of the plots on the right, that are each corresponding to a different EEG channel*

Appendix F

IBI related parameters

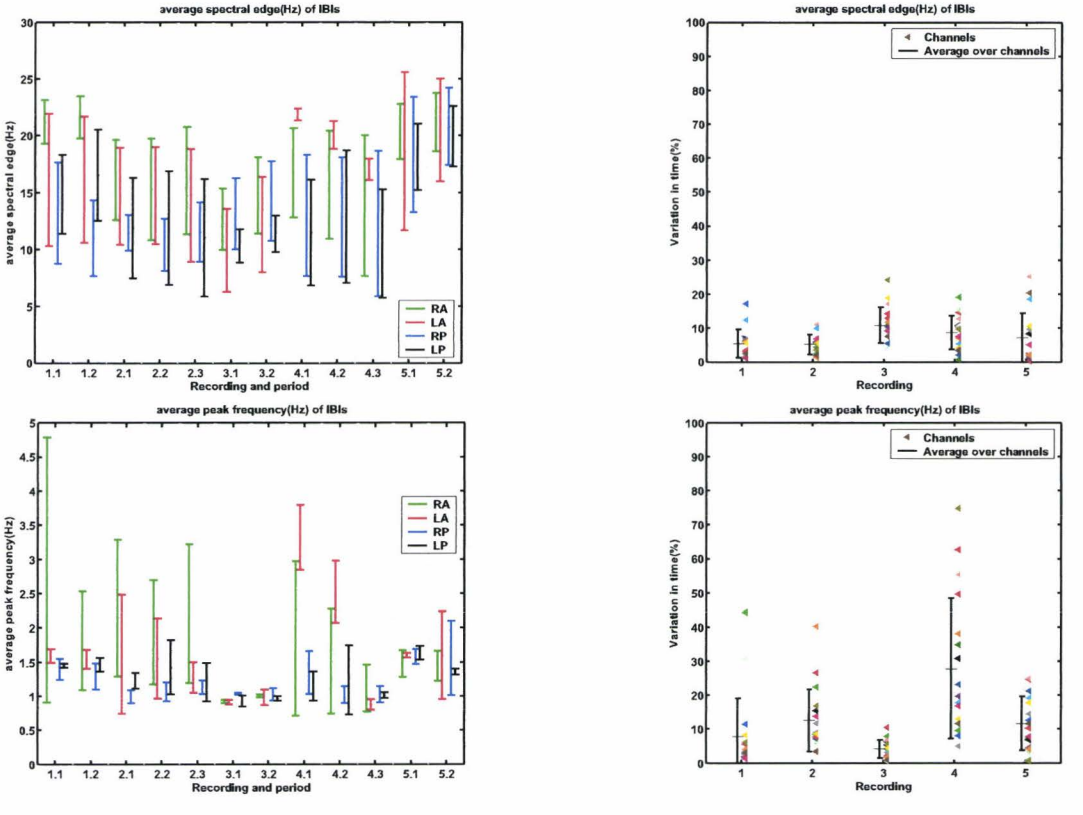

Figure F.1: *Parameters related to a specific frequency*

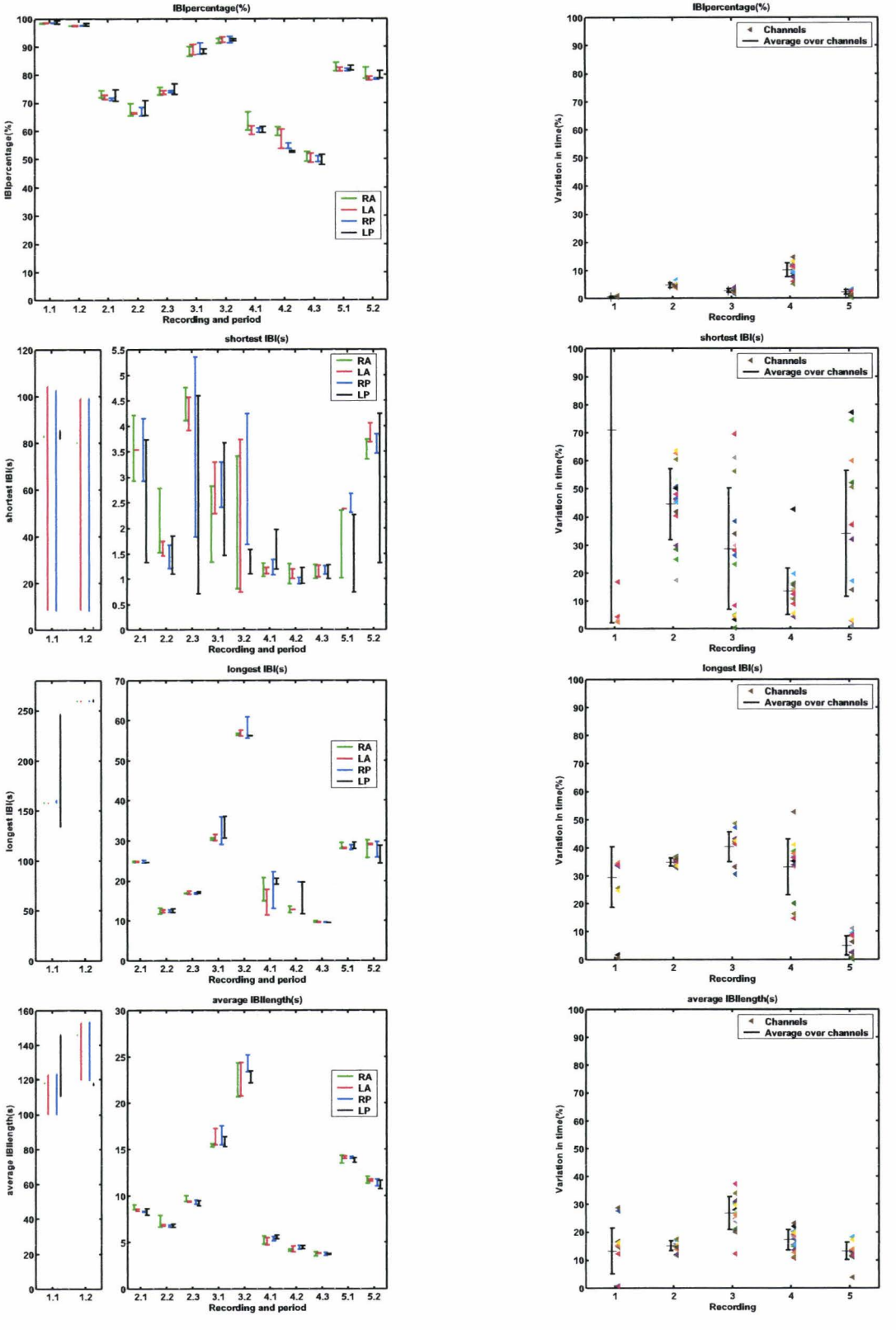

Figure F.2: *Time domain parameters*

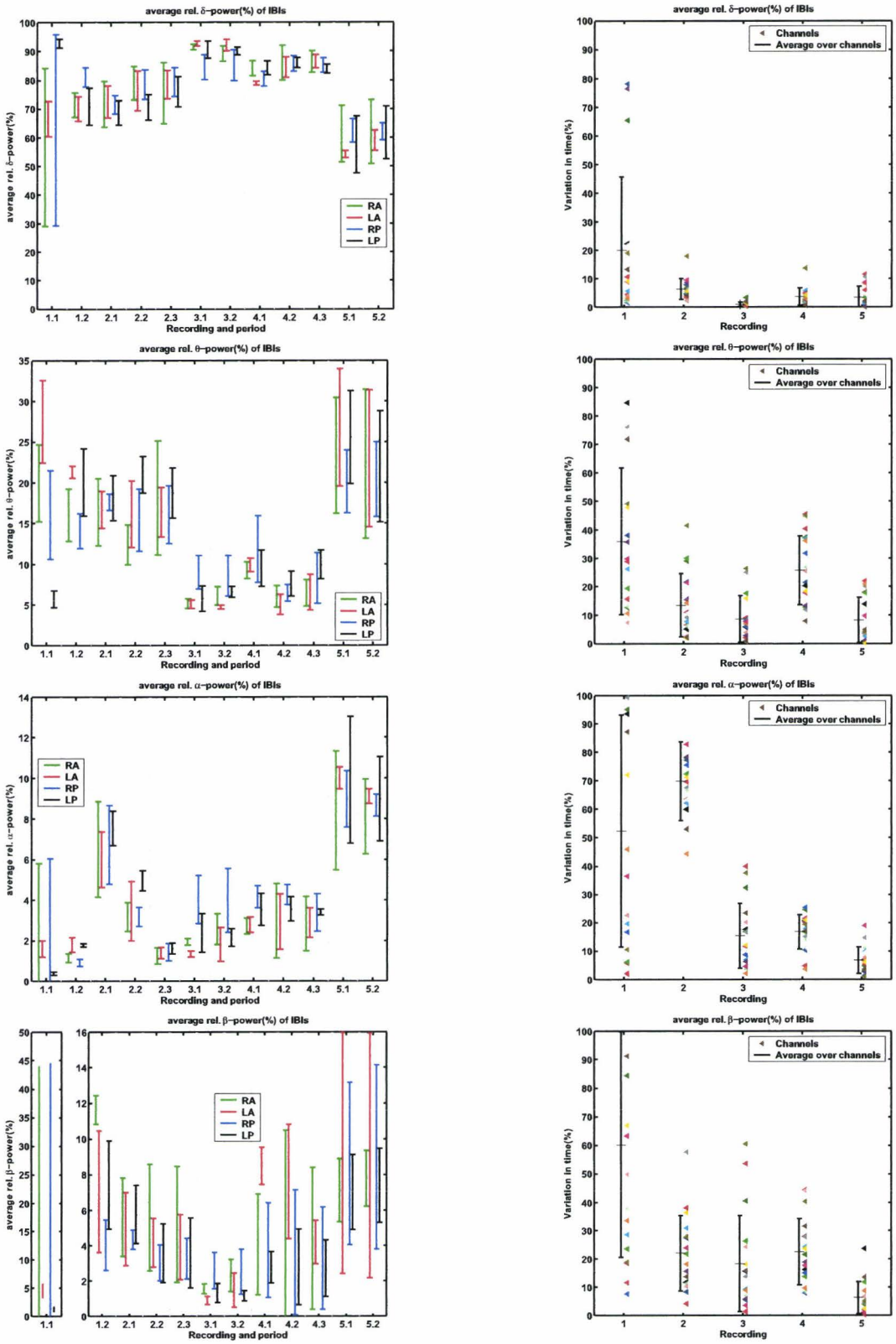

Figure F.3: *Relative power parameters*

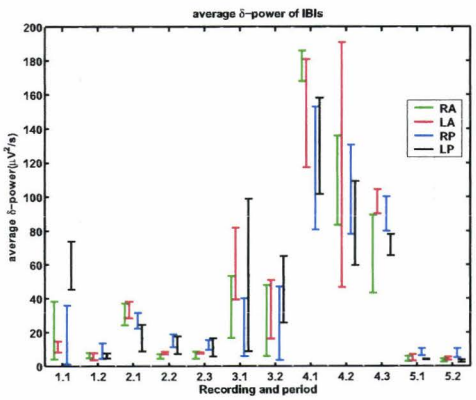
average δ-power of IBIs
average δ-power(μV²/s)
Recording and period
RA
LA
RP
LP

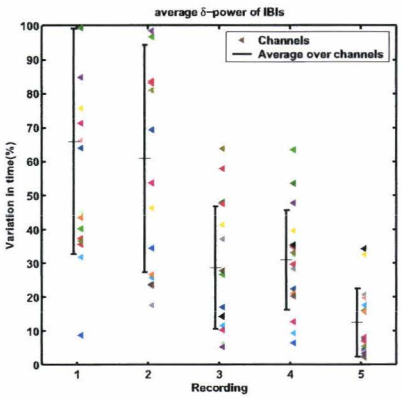
average δ-power of IBIs
Variation in time(%)
Recording
Channels
Average over channels

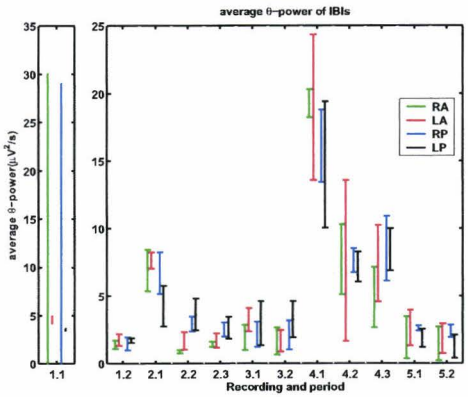
average θ-power of IBIs
average θ-power(μV²/s)
Recording and period
RA
LA
RP
LP

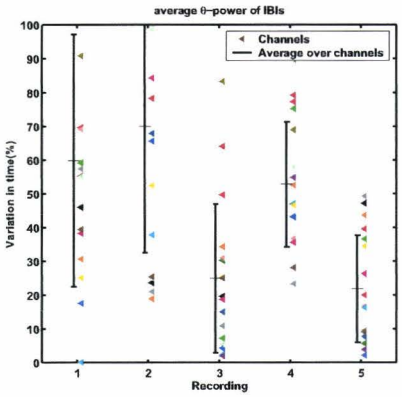
average θ-power of IBIs
Variation in time(%)
Recording
Channels
Average over channels

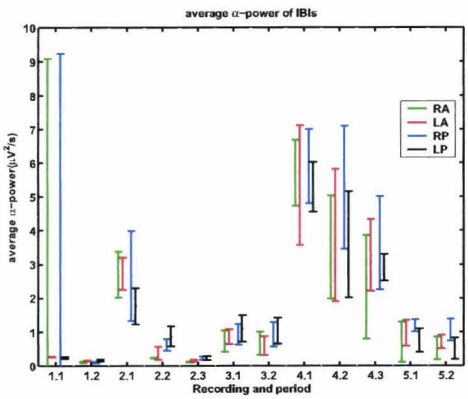
average α-power of IBIs
average α-power(μV²/s)
Recording and period
RA
LA
RP
LP

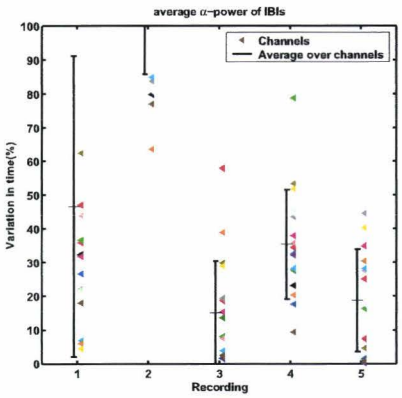
average α-power of IBIs
Variation in time(%)
Recording
Channels
Average over channels

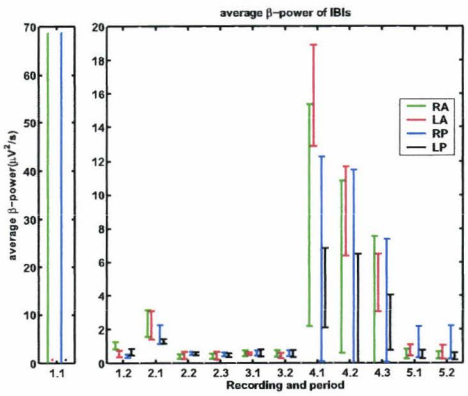
average β-power of IBIs
average β-power(μV²/s)
Recording and period
RA
LA
RP
LP

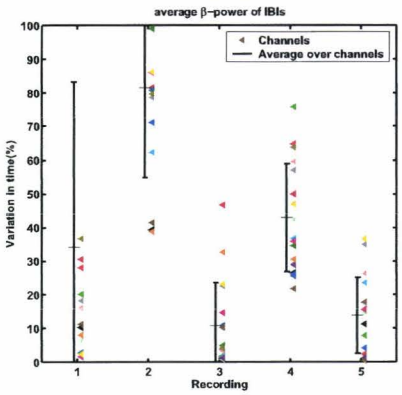
average β-power of IBIs
Variation in time(%)
Recording
Channels
Average over channels

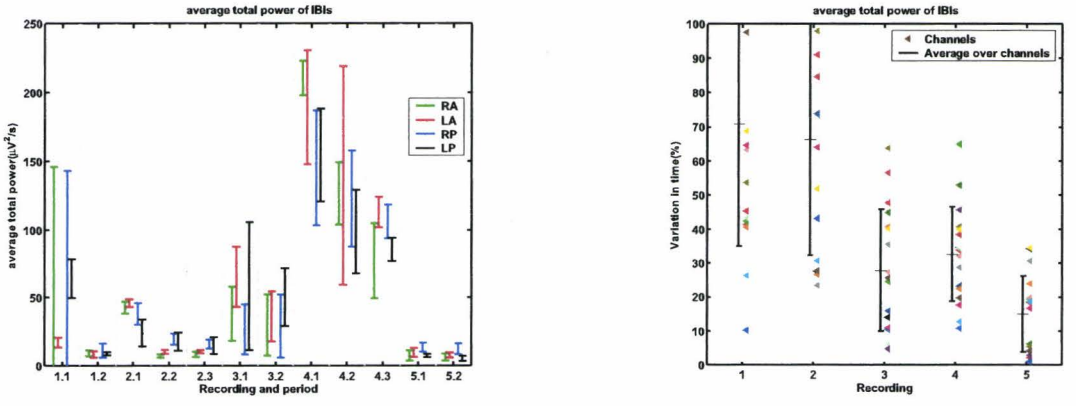

Figure F.4: *Absolute power parameters*

Bibliography

[1] Afdeling klinische neurofysiologie Academisch Ziekenhuis Nijmegen, *handleiding neonataal EEG*, Dec 1996

[2] E.Biagioni, L.Bartalena, A.Boldrini, R.Pieri, G.Cioni, *Constantly discontinuous EEG patterns in full-term neonates with hypoxic-ischaemic encephalopathy*, Clinical Neurophysiology 110:1510-1515, 1999

[3] C.Binnie, R.Cooper, F.Manguire, J.Osselton, P.Prior, B.Tedman, *Clinical Neurophysiology, Volume 2*, First edition, Elsevier, 2003

[4] P.J.M.Cluitmans, *Neuromonitoring*, Lecture Notes, University of Technology Eindhoven, 2002

[5] J.R.C.Conde, E.D.Martínez, C.G.Campo, A.M.Pérez, M.L.Mclean, *Positive temporal sharp waves in preterm infants with and without brain ultrasound lesions*, Clinical Neurophysiology 115:2479-2488, 2004

[6] G.Holmes, J.Rowe, J.Hafford, R.Schmidt, M.Testa, A.Zimmerman, *Prognostic value of the electroencephalogram in neonatal asphyxia*, Electroencephalography and Clinical Neurophysiology 53:60-72, 1982

[7] W.Kahle, M.Frotscher, G.Spitzer, *Atlas van de anatomie: Zenuwstelsel en zintuigen*, SESAM, 17th edition, 2000.

[8] V.H.J.M.van Kranen-Mastenbroek, *Het neonatale EEG: een (dis)continue zorg*, www.nvknf.nl/ onderwijs/nascholing/knfdagen/verslagen/2002/knfdagen2002kranen.htm#begin, 2002

[9] Nederlandse vereniging van laboranten klinische neurofysiologie, *nascholing EEG*, University Medical Center Utrecht, 8th of June 2001

[10] E.Niedermeyer, F.Lopes da Silva, *Electroencephalography: Basic principles, Clinical applications, and related fields*, Fifth Edition, Lippincott Williams & Wilkins, ISBN:0781751268, 2005

[11] D.Selton, M.Andre, J.M.Hascot, *Normal EEG in very premature infants: reference criteria*, Clinical Neurophysiology 111:2116-2124, 2000

[12] J.E.Stockard-Pope, R.G.Bickford, S.S.Berner, J.S.Curran, *Atlas of neonatal electroencephalography*, Second Edition, Raven Press, ISBN:0881678511, 1992

[13] M.Thordstein, A.Flisberg, N.Löfgren, R.Bågenholm, K.Lindecrantz, B.G.Wallin, L.Kjellmer, *Spectral Analysis of burst periods in EEG from healthy and post-asphyctic full-term neonates*, Clinical Neurophysiology 115:2461-2466, 2004

[14] S.N.the Tich, M.Vecchierini, T.Debillon, and Y.Pron, *Effects of Sufentanil on Electroencephalogram in Very and Extremely Preterm Neonates*, Pediatrics 111:123-128, 2003

[15] M.C.Toet, W.van der Meij, L.S.de Vries, C.S.P.M.Uiterwaal, K.C.van Huffelen, *Comparison Between Simultaneously Recorded Amplitude Integrated Electroencephalogram (Cerebral Function Monitor) and Standard Electroencephalogram in Neonates*, Pediatrics 109(5):772-779, May 2002

[16] S.Victor, R.E.Appleton, M.Beirne, A.G.Marson, and M.Weindling, *Spectral Analysis of Electroencephalography in Premature Newborn Infants: Normal Ranges*, Pediatric Research 57(3):336-341, 2005

[17] A.de Weerd, *Atlas of EEG: in the first months of life*, First Edition, Elsevier, 1995.

[18] G.B.Young, O.P.da Silva, *Effects of morphine on the electroencephalograms of neonates: a prospective observational study*, Clinical Neurophysiology 111:1955-1960, 2000

[19] http://butler.cc.tut.fi/ malmivuo/bem/bembook/00/co.htm

[20] http://www.colorado.edu/epob/epob1220lynch/image/figur5i.jpg

[21] http://www.mind.ilstu.edu